

Vintix: Action Model via In-Context Reinforcement Learning

Andrei Polubarov ^{*1 2 3} Nikita Lyubaykin ^{*1 4} Alexander Derevyagin ^{*1 5} Ilya Zisman ^{1 2 3} Denis Tarasov ¹
 Alexander Nikulin ^{1 6} Vladislav Kurenkov ^{1 4}

Abstract

In-Context Reinforcement Learning (ICRL) represents a promising paradigm for developing generalist agents that learn at inference time through trial-and-error interactions, analogous to how large language models adapt contextually, but with a focus on reward maximization. However, the scalability of ICRL beyond toy tasks and single-domain settings remains an open challenge. In this work, we present the first steps toward scaling ICRL by introducing a fixed, cross-domain model capable of learning behaviors through in-context reinforcement learning. Our results demonstrate that Algorithm Distillation, a framework designed to facilitate ICRL, offers a compelling and competitive alternative to expert distillation to construct versatile action models. These findings highlight the potential of ICRL as a scalable approach for generalist decision-making systems. Code to be released at dunnolab/vintix.

1. Introduction

The pursuit of generalist control and decision-making agents has long been a major target of the reinforcement learning (RL) research community (Sutton & Barto, 1998). These agents are envisioned to handle a diverse set of tasks while exhibiting adaptation properties such as self-correction and self-improvement based on reward functions. Notably, traditional online RL algorithms demonstrate these properties in narrow domains and can achieve exceptional performance (Berner et al., 2019; Badia et al., 2020; Schrittwieser et al., 2020; Baker et al., 2022; Team et al., 2023). However, their online nature of learning and frequent reliance on environment-specific training is still considered a challenge to overcome limiting the scalability (Dulac-Arnold et al.,

^{*}Equal contribution ¹AIRI ²Skoltech ³Research Center for Trusted Artificial Intelligence, ISP RAS ⁴Innopolis University ⁵HSE ⁶MIPT. Correspondence to: Vladislav Kurenkov <kurenkov@airi.net>. Work done by dunnolab.ai.

Proceedings of the 42st International Conference on Machine Learning, Vancouver, Canada. PMLR 267, 2025. Copyright 2025 by the author(s).

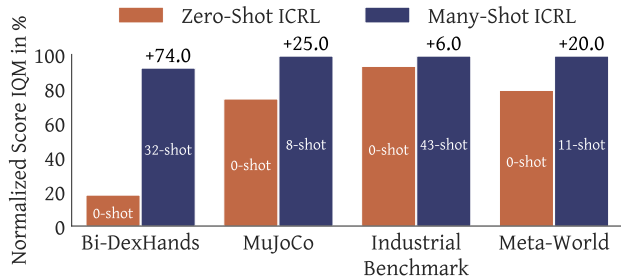


Figure 1. Vintix: Self-Correction with Many-Shot ICRL. Many-shot ICRL consistently self-corrects online on the training tasks (87) nearing the demonstrators’ performance across four domains. Optimal number of shots for many-shot ICRL are shown inside the bar for each task. One shot corresponds to one online episode. See Section 3 for more details and comparisons to action models based on expert distillation.

2019; Levine et al., 2020).

In contrast to online reinforcement learning, a recent boom of generative models, revitalized by Large Language Models and their emergent properties (Brown et al., 2020), sparked a high amount of interest in leveraging offline data for RL training: from specialized offline RL algorithms (Levine et al., 2020; Tarasov et al., 2024) to *Action Models* capable of handling many cross-domain tasks at the same time (Reed et al., 2022; Gallouédec et al., 2024; Haldar et al., 2024; Collaboration et al., 2024; Schmied et al., 2024; Sridhar et al., 2024).

Current approaches to pre-training cross-domain action models broadly fall into two categories. The first utilizes all available data, conditioning policies on return-to-go targets in a framework inspired by upside-down reinforcement learning principles (Schmidhuber, 2019; Lee et al., 2022; Schmied et al., 2024). The second, and currently dominant, approach prioritizes expert demonstrations, often disregarding reward signals entirely, as exemplified by Reed et al. (2022) and Haldar et al. (2024).

While the field increasingly steers toward language and demonstration-guided paradigms over reward-centric approaches, the “Reward is enough” principle (Silver et al., 2021) continues to offer a foundational framework for

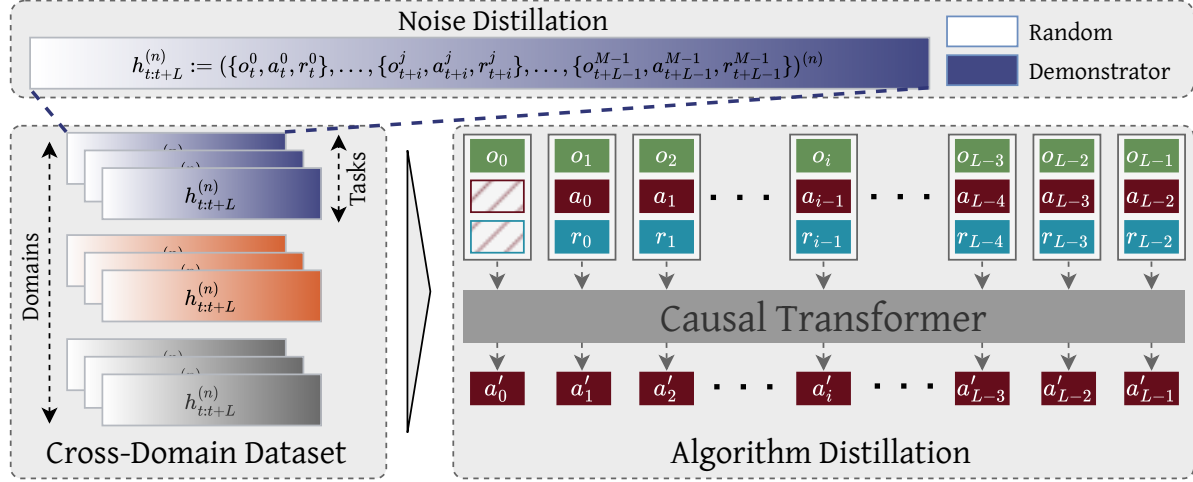


Figure 2. Vintix: Approach Overview. Stage 1 (Noise Distillation) - approximating policy improvement trajectory by injecting gradually annealed uniform noise (see Algorithm 1). Stage 2 (Cross-Domain Dataset) - combining collected multi-episodic sequences into shared cross-domain dataset for subsequent model training. Stage 3 (Algorithm Distillation) - running AD (Laskin et al., 2022) with collated $\{s, a, r\}$ triplets on collected dataset.

agents that learn to maximize arbitrary rewards through trial and error. This perspective has inspired methods like Algorithm Distillation (Laskin et al., 2022), which operationalizes reward-driven learning by training agents via next-token prediction over historical reinforcement learning (RL) trajectories — a mechanism that directly enables In-Context Reinforcement Learning (ICRL). Though initial implementations of this framework, alongside extensions such as by Zisman et al. (2024a;b); Sini et al. (2024); Nikulin et al. (2024), have been demonstrated only on toy and grid-based tasks within single domains, their data-driven origin positions them as a promising avenue for scaling reward-centric agents to broader, more complex environments.

In this work, we start an investigation into cross-domain action models through In-Context Reinforcement Learning (ICRL), grounded in the Algorithm Distillation framework (Laskin et al., 2022). By focusing on a data-centric approach to ICRL (summarized in Figure 2), we present Vintix, a multi-task action model that exhibits initial signs of inference-time self-correction on training tasks (Figure 1) and preliminary evidence of adaptation to parametric task variations (Section 3.3).

Our key contributions are as follows:

- **Continuous Noise Distillation** (Section 2.1): We propose a data collection strategy extending the work of Zisman et al. (2024a) to continuous action spaces to ease the collection of training data.
- **Open Tools and Datasets for ICRL** (Section 2.2): We publicly release datasets for 87 tasks across

four domains (Meta-World, MuJoCo, Bi-DexHands, Industrial-Benchmark), along with data collection tools and instrumentation to support the development of action models eliciting ICRL behavior.

- **Cross-Domain Scaling of ICRL** (Section 3): We empirically demonstrate that the proposed model, Vintix, can self-correct to attain demonstrator-level performance on training tasks (Figure 1) and adapt to controlled parametric task variations at inference-time.

2. Approach

At the core of our approach (Figure 2) is Algorithm Distillation (Laskin et al., 2022), a two-step Offline Meta-RL algorithm. The first step involves collecting ordered training histories from base reinforcement learning (RL) algorithms, while the second step involves a decoder-only transformer trained solely for the next-action prediction. This approach facilitates in-context learning by effectively distilling the policy improvement operator into a causal sequence model. We further propose two augmentations to this technique: (1) democratizing the data collection process by introducing a continuous extension of the noise-distillation procedure by Zisman et al. (2024a); (2) conducting generalist agent-style cross-domain training on the acquired dataset.

2.1. Continuous Noise Distillation

Collecting learning histories can be time-consuming and computationally expensive, as it requires curated learning histories of RL algorithms for each task individually. The

resulting trajectories may be excessively long due to poor sample efficiency and may exhibit noise due to training instabilities. Recently, [Zisman et al. \(2024a\)](#) demonstrated that learning trajectories approximated through noise distillation can facilitate the emergence of in-context learning capabilities via next-action prediction. In this framework, called AD^ϵ , policy improvement is approximated by gradually reducing the proportion of random noise injected into the demonstrator policy during its execution in the environment. More specifically, at each time step, a random action is selected with probability ϵ , while a demonstrator action is chosen with probability $1 - \epsilon$. ϵ is annealed throughout the trajectory, starting at $\epsilon = 1$ (random policy) at the beginning and gradually decreasing to $\epsilon = 0$ (demonstrator policy) by the end.

The AD^ϵ data collection strategy was originally designed for discrete action spaces. In our work, we propose its extension to continuous action spaces, where the resulting action is defined as a linear mixture of uniform random noise and demonstrator actions. This contrasts with [Brown et al. \(2019\)](#), who employed an epsilon-greedy approach that alternates between fully random and fully expert actions with probability ϵ . The pseudo-code for our noise-distillation procedure is formalized in Algorithm 1.

Algorithm 1 Noise distillation for continuous action spaces

Require: Demonstrator policy π_D , task environment, noise schedule \mathcal{E} , number of time steps in the trajectory T , trajectory buffer \mathcal{D} , action space lower and upper bounds a_{min}, a_{max}

- 1: Sample s_0 from task environment
- 2: **for** $t \in T$ **do**
- 3: Noise magnitude: $\epsilon_i = \mathcal{E}(t)$
- 4: Noise: $u \sim Uniform(a_{min}, a_{max})$
- 5: Current action: $a_i = (1 - \epsilon_i) * \pi_D(s_i) + \epsilon_i * u$
- 6: Obtain $\{s_{i+1}, r_i, t_i\}$ by executing a_i in task environment
- 7: Append $\{s_i, a_i, s_{i+1}, r_i, t_i\}$ to \mathcal{D}
- 8: **end for**

The noise schedule \mathcal{E} plays a crucial role in the generation of training trajectories. We observed that linear annealing of ϵ often results in non-smooth trajectories with abrupt transitions from random to demonstrator performance. This effect can negatively impact the model’s convergence; therefore, careful tuning of the noise schedule was necessary for certain tasks. A more detailed description of the epsilon decay functions is provided in the Appendix A.3. Figure 3 illustrates that Algorithm 1 generates trajectories with smooth reward curves, closely resembling the learning histories observed in [Zisman et al. \(2024a\)](#). For Task-Level dataset visualization please refer to Appendix E.

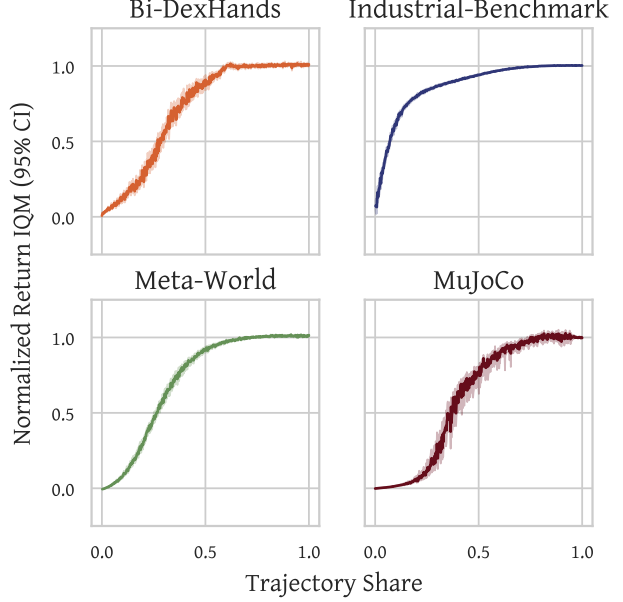


Figure 3. Continuous Noise Distillation trajectories. Aggregated normalized returns for the collected cross-domain dataset. Returns are normalized with respect to random and demonstrator scores, while trajectory lengths are reported as a fraction of their maximum values.

2.2. Cross-Domain Dataset

Building upon Continuous Noise Distillation method, we then collect a cross-domain dataset. Our dataset consists of environments with continuous N -dimensional vector observations and continuous multi-dimensional actions. This focus was chosen to isolate the challenge of processing multi-modal inputs from the challenge of inference-time adaptation across different tasks and domains, allowing us to concentrate on the latter. The collected cross-domain dataset consists of 87 distinct tasks spanning across four domains:

1. **MuJoCo** ([Todorov et al., 2012](#)) - classical multi-joint dynamics control suite containing 11 various tasks with different state-action spaces and reward functions.
2. **Meta-World** ([Yu et al., 2021](#)) - benchmark for Multi-Task and Meta RL containing 45 manipulation tasks with shared state and action structure.
3. **Bi-DexHands** ([Chen et al., 2022](#)) - benchmark simulator that includes 15 diverse tasks focused on dexterous manipulation.
4. **Industrial-Benchmark** ([Hein et al., 2017](#)) - benchmark featuring synthetic continuous control tasks that simulate the properties of real industrial problems.

Train Dataset				
Domain	Tasks	Episodes	Timesteps	Sample Weight
Bi-DexHands	15	216k	31,7M	14,2%
Industrial-Benchmark	16	96k	24M	10,8%
Meta-World	45	670k	67M	30,1%
MuJoCo	11	665k	100M	44,9%
Overall	87	1,6M	222,7M	100%

Table 1. Cross-Domain Dataset summary. Aggregation is performed by summing all transitions (in the form of $\{s_i, a_i, s_{i+1}, r_i, t_i\}$) across all trajectories collected for all tasks. Detailed dataset statistics can be found ad Section G

Table 1 contains detailed statistics of the training dataset. More detailed information on datasets can be found in the Appendix A.

Training Demonstrators For MuJoCo and Meta-World we utilized demonstrator policies provided in JAT (Gal-louédec et al., 2024). However, for several tasks within Meta-World, we trained our own demonstrators due to the unsatisfactory performance of the provided experts. Bi-DexHands demonstrators were trained using official PPO (Schulman et al., 2017) implementation with an increased number of parallel environments. The demonstrator policies for the Industrial Benchmark were trained using the provided scripts, which were built on top of the Stable-Baselines 3 library (Raffin et al., 2021). In-depth view of demonstrators performance can be found in the Appendix H.

2.3. Training and Inference Pipeline

The input data consists of a set of multi-episodic subsequences sampled from the original noise-distilled trajectories, formalized as follows:

$h_{t:t+L}^{(n)} := (\{o_t^0, a_t^0, r_t^0\}, \dots, \{o_{t+i}^j, a_{t+i}^j, r_{t+i}^j\}, \dots, \{o_{t+L-1}^{M-1}, a_{t+L-1}^{M-1}, r_{t+L-1}^{M-1}\})^{(n)}$. Where t is the index of the sub-sequence's starting point within the full noise-distilled trajectory, L is the length of the sub-sequence, M denotes the total number of episodes within the sub-sequence, which varies due to differing episode lengths across tasks, $i \in [0, L - 1]$ is a lower subscript timestamp index within the sub-sequence, $j \in [0, M - 1]$ is an upper subscript episode index within the sub-sequence. The global subscript n identifies a unique task, which is uniformly sampled from a multi-domain dataset, defined as: $\mathcal{M}_n = \bigcup_{d=1}^D \mathcal{M}_{n_d}^d$, where $d \in [1, D]$ represents the domain identifier, and n_d denotes the task belonging to the respective domain. The overall data pipeline closely resembles that of Laskin et al. (2022), with the only difference being its cross-domain coverage.

2.3.1. MODEL ARCHITECTURE

At a high level, Vintix consists of three main components: an encoder, which maps raw input sequences $h_{t:t+L}^{(n)}$ into a fixed-size embedding space; a transformer backbone, which processes the encoded inputs; and a decoder, which maps the hidden states produced by the transformer back to the original action space.

All input sequences $h_{t:t+L}^{(n)}$ are split into groups based on observation and action space dimensionalities. For each group, a separate encoder and decoder MLP head are created, enabling the model to map variable observation and action spaces into a shared embedding space. It is important to note that the model is task-agnostic in the sense that it has access only to the dimensionality-based group identifier, but not to an individual task identifier. While the task identifier is a unique ID assigned to each task in the dataset, the group identifier simply indicates whether a set of tasks shares the same observation and action space dimensions, as well as the semantic meaning of each channel.

In contrast to Laskin et al. (2022), which processes each entity in the sequence $h_{t:t+L}^{(n)}$ as a separate token, we stack the representations of the previous action, previous reward, and current observation into a single sequence token. This approach is consistent with token alignment methods proposed by Duan et al. (2016); Grigsby et al. (2024a;b). Such design choice allowed us to significantly expand the context window size by compressing its representation by a factor of three.

In summary, Vintix is a 300M-parameter next-action prediction model with 24 layers, 16 heads, an embedding size of 1024, and a post-attention feed-forward hidden size of 4096. TinyLLama (Zhang et al., 2024) was chosen as the transformer backbone for the Vintix model.

2.3.2. TRAINING

The input batches are created by collating together multiple input sequences $h_{t:t+L}^{(n)}$. To standardize the data across tasks, rewards are scaled by task-specific factors (see Appendix G), and observations are normalized. This procedure significantly enhances model performance by reducing task distinguishability based on raw input values, thereby encouraging the model to rely on contextual information to infer the task.

Afterward, sequences are processed by the corresponding encoders to obtain fixed-size representations. The sequence of representations is then passed into a transformer, whose outputs are subsequently decoded into predicted actions a_{pred} . The training objective is to minimize the Mean Squared Error loss between the predicted actions a_{pred} and the ground-truth trajectory actions a_{true} . Training is conducted on 8

H100 GPUs with a batch size of 64 and 2 gradient accumulation steps. The input sequence length L is set to 8192. For more detailed hyperparameter information, refer to Appendix D.

2.3.3. INFERENCE

Model inference is performed iteratively, starting with an empty context. The model generates the first action based on the initial observation and subsequently receives the next observation and reward. Each new transition tuple is appended to the context. When the context exceeds its maximum length L , the oldest token is removed, effectively implementing a sliding attention window (Beltagy et al., 2020). To accelerate inference, we utilized the KV-cache implementation from the FlashAttention library (Dao et al., 2022). Since absolute positional encodings are incompatible with sliding attention window with KV-caching due to positional drift, we employed ALiBi encodings (Press et al., 2022), which are inherently relative in nature.

3. Results

3.1. Inference-Time Self-Correction on Training Tasks

First, we aim to verify whether the Vintix model has the capability for context-based inference-time adaptation through self-correction. To achieve this, we deploy the model on training tasks (ML45 split for Meta-World, ML20 split for Bi-DexHands and setpoints $p \in [0, 75]$ for Industrial-Benchmark) by iteratively unrolling its actions in a cold-start manner, beginning with an empty initial context. Figure 4 illustrates that the model progressively improves its policy in each domain as the number of shots (episodes played) increases. The agent starts with a suboptimal performance and gradually self-corrects by inferring task-related information from the accumulated context, ultimately reaching near-demonstrator-level performance.

Notably, this improvement is both progressive and consistent along the shots-made axis and is observed across multiple domains with varying dynamics and morphology. For task-level graphs depicting inference-time performance with an empty context, refer to Section F.

This behavior suggests that, despite being task-agnostic, the model can infer environment’s implicit structure and utilize it to enable self-corrective adaptation across training tasks.

3.2. Comparison to Related Action Models

Next, we aim to assess the performance of Vintix compared to other generalist agents trained across multiple domains and determine whether its self-corrective inference provides an advantage in matching demonstrator performance levels.

To verify this, we compare the average demonstrator-

normalized performance of Vintix with that of Gallouédec et al. (2024) and Sridhar et al. (2024) across training tasks in overlapping domains (MuJoCo and Meta-World). JAT and REGENT scores are taken directly from the respective papers. For Vintix, we extract the average performance over 100 episodes after reaching inference-time convergence (i.e., achieving the best k -shot performance per task).

Since most of our demonstrators were sourced from JAT - and REGENT also adopted random and expert scores from JAT - the comparison of normalized scores is valid. However, we improved expert performance for several tasks by fine-tuning hyperparameters and normalized our raw returns with respect to these newly enhanced scores. This adjustment lowers our normalized performance relative to JAT and REGENT, but we adopted this comparison approach as our initial focus is on evaluating the agent’s ability to match demonstrator performance rather than comparing absolute scores.

Figure 5 illustrates that inference-time self-correction enables Vintix to outperform JAT and REGENT on Meta-World and MuJoCo by significant margins. More detailed comparison can be found in Section I. These results may further highlight a fundamental advantage of Algorithm Distillation over Expert Distillation, namely its adaptability, as initially reported in Laskin et al. (2022).

3.3. Generalization Analysis

In this subsection, we take a closer look at the models performance in regards to both unseen parametric variations and tasks.

Generalization to Parametric Variations

Further experiments aim to assess whether the Vintix model is capable for context-based inference-time adaptation to task variations that were not encountered during training.

To evaluate this, we performed the cold-start inference procedure described in previous sections on a set of MuJoCo environments with unobservable variations in viscosity and gravity, which were also unseen during training (for more details on MuJoCo parameter variations, refer to Section A.2.1). Additionally, we applied the same procedure to unseen environments in the Industrial-Benchmark domain (setpoint $p \in [80, 100]$, see Section A.2.4).

Figure 6 presents the experimental results. As shown, Vintix is still able to achieve near-demonstrator performance in modified environments across both domains. However, a slight decline in convergence quality is observed—slower convergence speed in MuJoCo and subtly diminished asymptotic performance in Industrial-Benchmark. The slower convergence rate suggests that the model requires more iterations of self-correction to reach demonstrator-level policy

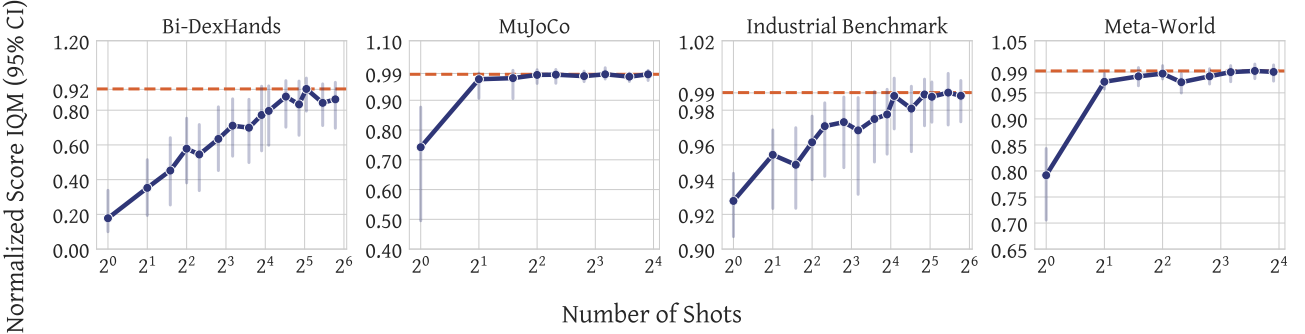


Figure 4. Dynamic self-correction with Many-Shot ICRL. The model’s actions are executed iteratively in the environment without any initial context or task identifier provided to the agent (i.e., cold start). Although it starts with a suboptimal policy, the model gradually improves through context-based self-correction. Results are aggregated over training tasks (ML45 split for Meta-World, ML20 split for Bi-DexHands and setpoints $p \in [0, 75]$ for Industrial-Benchmark) within each domain.

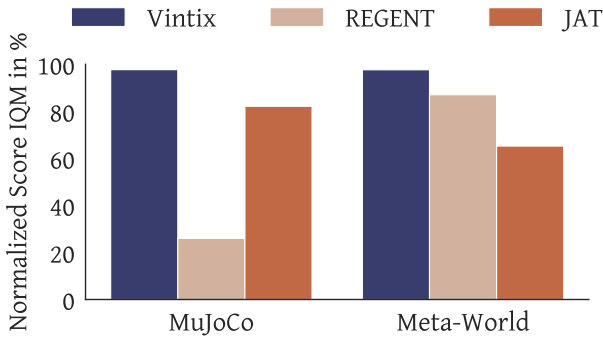


Figure 5. Average domain-level demonstrator-normalized returns on training tasks: Vintix vs. REGENT vs. JAT. JAT and REGENT scores are taken directly from the respective papers, while for Vintix, we analyze 100 episodes after reaching inference-time convergence.

in environments with moderate parametric variations.

Generalization to New Tasks

Finally, we evaluate Vintix’s performance on entirely new tasks that were not seen during training to determine whether it can perform in-context reinforcement learning by inferring task structure in this challenging setting.

As in the previous experiments, we unroll actions from Vintix with no initial context on test tasks from the Meta-World ML45 split and the Bi-DexHands ML20 split (Section A.2). Overall, we observed that Vintix is not yet capable to handle significantly new tasks. Figure 7 presents one successful rollout and one failure case for each domain (for detailed task-level results, refer to Section F). On the *Door-Unlock* task from Meta-World, Vintix achieved 47% of the mean expert-normalized score, while on the *Door-Open-Inward* task from Bi-DexHands, it consistently maintained 31% of demonstrator performance. In failure scenarios, the model

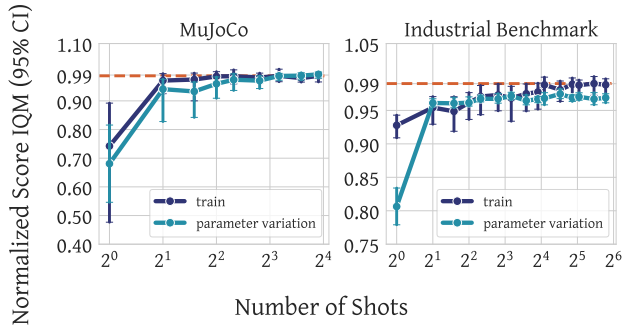


Figure 6. Cold-start many-shot inference procedure on tasks with parameter variations compared to training tasks. In MuJoCo, variations include changes in viscosity (0.05 and 0.1 vs. the original 0) and gravity ($\pm 10\%$). For the Industrial-Benchmark, we evaluate the model on previously unseen setpoint values, $p \in [80, 100]$.

exhibited random-level performance on the *Bin-Picking* task and performed below the random baseline on the *Hand-Kettle* task.

This observation aligns with our intuition and existing research in in-context RL, where even in toy task settings, such as those studied by Laskin et al. (2022); Sinii et al. (2024); Zisman et al. (2024a), authors employed significantly larger task sets in their experiments. Nevertheless, we believe this result is still promising as Vintix manages to demonstrate inference-time improvement through trial and error on certain tasks, despite being trained on only 87 distinct tasks.

4. Related Work

In-Context Learning. In-Context learning is often used to describe the capacity of large language models to adapt to new tasks after the training phase (Brown et al., 2020;

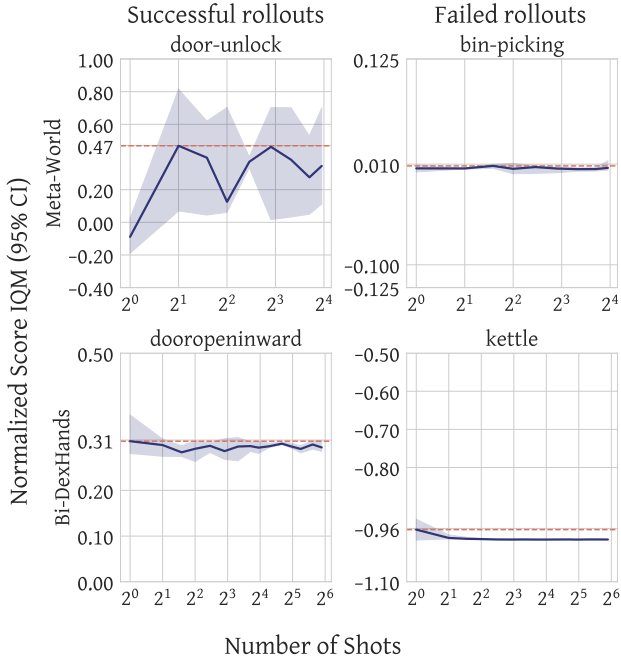


Figure 7. Inference-time performance on new tasks. One successful rollout and one failure case are reported for both Meta-World and Bi-DexHands. Inference is performed without an initial context in a task-agnostic manner.

Liu et al., 2021). In essence, in-context learning refers to an approach where the algorithm is provided with a set of demonstrations at test time, enabling it to infer task-related information (Min et al., 2022). In contrast, the in-weights paradigm typically relies on fine-tuning the model on downstream tasks (Finn et al., 2017; Wang et al., 2024; Ying et al., 2024). Compared to in-weights learning, in-context learning is gradient-free at deployment, which theoretically allows for a significant reduction in computational costs and facilitates the development of foundational models as a service, applicable to a broad range of real-world tasks (Sun et al., 2022; Dong et al., 2024). In our work, we use the many-shot in-context learning setup (Agarwal et al., 2024) with a large context window to the reinforcement learning framework.

Offline Memory-Based Meta-RL. Meta-reinforcement learning (Meta-RL) focuses on enabling agents to adapt to new tasks, environments, or dynamics through interaction experience. Numerous diverse approaches exist within the field of Meta-RL (Beck et al., 2024). At a high level, Meta-RL algorithms can be broadly categorized into two main segments: those explicitly conditioned on a task representation (Espeholt et al., 2018; Rakelly et al., 2019; Zhao et al., 2020; Sodhani et al., 2021) and those that infer task dynamics and reward functions from past experience often referred to as "In-Context". Implicit memory-based Meta-

RL can itself be divided into two major branches: a set of approaches inheriting from RL² (Duan et al., 2016) which encodes task-related information using the RNN's hidden state and directly leverages RL off-policy updates, including more recent transformer-based variants like AMAGO-{1, 2} (Grigsby et al., 2024a;b) and RELIC (Elawady et al., 2024). Another perspective on in-context reinforcement learning formalizes the training of a Meta-RL agent as an imitation learning problem. This can involve cloning optimal actions, as seen in methods like DPT (Lee et al., 2023), leveraging demonstrator's trajectories, as in ICRT (Fu et al., 2024), or utilizing the entire RL algorithm's learning history or its approximations derived via noise distillation (Zisman et al., 2024a). Examples of this data-centric approach include AD and its derivatives (Laskin et al., 2022; Kirsch et al., 2023; Sinii et al., 2024; Nikulin et al., 2024). Our algorithm is most closely aligned with the last described category and represents a multi-domain AD trained on trajectories obtained through noise distillation.

Multi-Task Learning. Multi-Task Learning (MTL) can be formalized as a paradigm of joint multi-task optimization, aiming to maximize positive knowledge transfer (synergy) between tasks while minimizing detrimental task interference. Numerous studies explore Multi-Task Learning (MTL) beyond the naive minimization of the sum of individual task losses, a method commonly referred to as unitary scalarization. Significant efforts have been made in the fields of massively multilingual translation, where each language pair is treated as a separate task (McCann et al., 2018; Radford et al., 2019; Wang et al., 2020; Li & Gong, 2021), as well as in reinforcement learning (Espeholt et al., 2018; Hessel et al., 2018; Sodhani et al., 2021; Kumar et al., 2023) and robotics (Wulfmeier et al., 2020; Wang et al., 2024). The most common solutions include various types of gradient surgeries to minimize negative interactions between different tasks (Wang et al., 2020; Yu et al., 2020), adaptive tuning of task weights (Sener & Koltun, 2019; Li & Gong, 2021), scaling of model size, and temperature tuning (Shaham et al., 2023). It is also worth noting that several studies argue there is no substantial evidence that specialized multi-task optimizers consistently outperform unitary scalarization, while also introducing significant complexity and computational overhead (Xin et al., 2022; Kurin et al., 2023). It is important to note that the aforementioned works on Multi-Task RL rely on various forms of explicit task conditioning, while our approach follows a task-agnostic paradigm that implicitly infers task-related information from interaction experience.

Generalist Agents and Large Action Models. Although most experiments in the field of meta-reinforcement learning (Meta-RL) are typically confined to a single domain of tasks (Duan et al., 2016; Anand et al., 2021; Laskin et al., 2022),

generalist agents aim to perform cross-domain training, often integrating multiple data modalities (Gallouédec et al., 2024; Reed et al., 2022). Primary advances in this area of research have been made in the field of robotic locomotion and manipulation, where researchers aim to develop generalizable policies and facilitate cross-domain knowledge transfer. This approach seeks to reduce the computational complexity of training policies for robotic applications. The renaissance of generalist robot policies has been notably driven by the availability of large open-source multi-domain robotic datasets like Open X-Embodiment (Collaboration et al., 2024). A variety of models build upon the foundations established by the Open X datasets, including RT-X (Collaboration et al., 2024), RT-1 (Brohan et al., 2023), Octo (Team et al., 2024), OpenVLA (Kim et al., 2024), DynaMo (Cui et al., 2024). Another category of models relies primarily on training data derived from simulated environments, with notable examples including JAT (Gallouédec et al., 2024), Gato (Reed et al., 2022) and Baku (Haldar et al., 2024). Other closely related work is by Sridhar et al. (2024), where authors propose a retrieval-based algorithm for in-context imitation in the presence of demos for new tasks. Although our work closely aligns with the field of generalist agents and works mentioned, our primary focus is on inference-time learning through trial and error driven by the data-centric approach.

Learned Optimizers. In contrast to traditional optimizers that follow hand-crafted update rules, learned optimizers employ a parameterized update rule that is meta-trained to optimize various objective functions (Li & Malik, 2016; Andrychowicz et al., 2016; Metz et al., 2020; Almeida et al., 2021). Thus, learned optimization can be seen as an alternative perspective on meta-learning (learning-to-learn), with recent approaches scaling to a wide range of tasks and requiring thousands of TPU-months for training (Metz et al., 2022). However, due to the non-stationarity and high stochasticity of the temporal difference (TD) objective, learned optimizers fail in reinforcement learning setting (Metz et al., 2022). To address these challenges, Optim4RL introduces RL-specific inductive bias (Lan et al., 2024), while OPEN enhances exploration by leveraging learnable stochasticity (Goldie et al., 2024). Both works can be considered optimization-centric approaches to Meta-RL, whereas we adopt a context-based approach.

Sequence Modeling in RL. With the increasing use of Transformers for modeling sequential data, several concurrent works (Chen et al., 2021; Janner et al., 2021) reformulated the Markov Decision Process as a causal sequence modeling problem. Chen et al. (2021) focused on reward conditioning and treated each component of the MDP as a separate token, while Janner et al. (2021) applied beam search over discretized states, actions, and rewards.

Subsequent research has expanded this direction by encouraging such models to maximize returns (Zhuang et al., 2024), adapting Decision Transformers to online learning settings (Zheng et al., 2022), and replacing the Transformer backbone with architectures that scale more efficiently with input length, such as Mamba (Huang et al., 2024).

Another line of work has aimed to scale this modeling paradigm to multi-domain and multi-modal environments (Reed et al., 2022; Gallouédec et al., 2024), or to leverage the in-context learning capabilities of Transformers for Meta-RL (Laskin et al., 2022; Lee et al., 2023). This latter direction is most closely related to Vintix, which is a memory-based, cross-domain Meta-RL method.

5. Conclusion and Future Work

The development of generalist reinforcement learning agents that adapt across domains remains a critical challenge, as traditional online RL methods—despite their success in narrow settings—face scalability limitations due to their reliance on environment-specific, interactive training (Dulac-Arnold et al., 2019; Levine et al., 2020). While recent advances in offline RL and generative action models have expanded the potential for data-driven learning, these approaches often prioritize expert demonstrations or language conditioning over reward-centric adaptation (Reed et al., 2022; Gallouédec et al., 2024; Haldar et al., 2024; Collaboration et al., 2024; Schmied et al., 2024; Sridhar et al., 2024). In this work, we explored an alternative paradigm rooted in In-Context Reinforcement Learning (ICRL), building on Algorithm Distillation (Laskin et al., 2022) to create agents that learn adaptive behaviors by a straightforward next-action prediction of learning histories or their proxies.

Our proposed approach and model, Vintix, demonstrates that ICRL can extend beyond prior single-domain, grid-based benchmarks. By introducing Continuous Noise Distillation, we ease the data collection process inherent to Algorithm Distillation and release a suite of datasets and tools for 87 tasks across four domains, which we hope would be helpful in community efforts toward scalable, cross-domain action models capable of in-context reinforcement learning. Empirically, we show that Vintix exhibits self-correction on training tasks and adapt to moderate controlled parametric variations without requiring gradient updates at inference time. These results, though preliminary and confined to structured settings, suggest that reward-guided ICRL provides a viable pathway for agents to autonomously refine their policies in response to environmental feedback.

While we believe the obtained results are promising, there is a large room for improvement as challenges remain in increasing the number of domains, developing more task-agnostic architectures that would allow not only for robust

self-correction but vital generalization to unseen tasks and self-improvement beyond demonstrators' performance. We hope this work encourages further investigation into data-centric, reward-driven frameworks for cross-domain RL agentic systems.

Impact Statement

This proposed model is strictly limited to the simulated environments used for evaluation due to its architectural limitations, and therefore does not present any safety concerns. However, in case one would like to finetune it for real-world purposes, it does not guarantee any sort of safe behavior and cautions must be made on the part of the user.

References

Agarwal, R., Singh, A., Zhang, L. M., Bohnet, B., Rosias, L., Chan, S., Zhang, B., Anand, A., Abbas, Z., Nova, A., Co-Reyes, J. D., Chu, E., Behbahani, F., Faust, A., and Larochelle, H. Many-shot in-context learning, 2024. URL <https://arxiv.org/abs/2404.11018>.

Almeida, D., Winter, C., Tang, J., and Zaremba, W. A generalizable approach to learning optimizers, 2021. URL <https://arxiv.org/abs/2106.00958>.

Anand, A., Walker, J., Li, Y., Vértes, E., Schrittwieser, J., Ozair, S., Weber, T., and Hamrick, J. B. Procedural generalization by planning with self-supervised world models, 2021. URL <https://arxiv.org/abs/2111.01587>.

Andrychowicz, M., Denil, M., Gomez, S., Hoffman, M. W., Pfau, D., Schaul, T., Shillingford, B., and de Freitas, N. Learning to learn by gradient descent by gradient descent, 2016. URL <https://arxiv.org/abs/1606.04474>.

Badia, A. P., Piot, B., Kapturowski, S., Sprechmann, P., Vitvitskyi, A., Guo, Z. D., and Blundell, C. Agent57: Outperforming the atari human benchmark. In *International conference on machine learning*, pp. 507–517. PMLR, 2020.

Baker, B., Akkaya, I., Zhokov, P., Huizinga, J., Tang, J., Ecoffet, A., Houghton, B., Sampedro, R., and Clune, J. Video pretraining (vpt): Learning to act by watching unlabeled online videos. *Advances in Neural Information Processing Systems*, 35:24639–24654, 2022.

Beck, J., Vuorio, R., Liu, E. Z., Xiong, Z., Zintgraf, L., Finn, C., and Whiteson, S. A survey of meta-reinforcement learning, 2024. URL <https://arxiv.org/abs/2301.08028>.

Beltagy, I., Peters, M. E., and Cohan, A. Longformer: The long-document transformer, 2020. URL <https://arxiv.org/abs/2004.05150>.

Berner, C., Brockman, G., Chan, B., Cheung, V., Dębiak, P., Dennison, C., Farhi, D., Fischer, Q., Hashme, S., Hesse, C., et al. Dota 2 with large scale deep reinforcement learning. *arXiv preprint arXiv:1912.06680*, 2019.

Brockman, G., Cheung, V., Pettersson, L., Schneider, J., Schulman, J., Tang, J., and Zaremba, W. Openai gym, 2016. URL <https://arxiv.org/abs/1606.01540>.

Brohan, A., Brown, N., Carbajal, J., Chebotar, Y., Dabis, J., Finn, C., Gopalakrishnan, K., Hausman, K., Herzog, A., Hsu, J., Ibarz, J., Ichter, B., Irpan, A., Jackson, T., Jesmonth, S., Joshi, N. J., Julian, R., Kalashnikov, D., Kuang, Y., Leal, I., Lee, K.-H., Levine, S., Lu, Y., Malla, U., Manjunath, D., Mordatch, I., Nachum, O., Parada, C., Peralta, J., Perez, E., Pertsch, K., Quiambao, J., Rao, K., Ryoo, M., Salazar, G., Sanketi, P., Sayed, K., Singh, J., Sontakke, S., Stone, A., Tan, C., Tran, H., Vanhoucke, V., Vega, S., Vuong, Q., Xia, F., Xiao, T., Xu, P., Xu, S., Yu, T., and Zitkovich, B. Rt-1: Robotics transformer for real-world control at scale, 2023. URL <https://arxiv.org/abs/2212.06817>.

Brown, D. S., Goo, W., and Niekum, S. Better-than-demonstrator imitation learning via automatically-ranked demonstrations, 2019. URL <https://arxiv.org/abs/1907.03976>.

Brown, T. B., Mann, B., Ryder, N., Subbiah, M., Kaplan, J., Dhariwal, P., Neelakantan, A., Shyam, P., Sastry, G., Askell, A., Agarwal, S., Herbert-Voss, A., Krueger, G., Henighan, T., Child, R., Ramesh, A., Ziegler, D. M., Wu, J., Winter, C., Hesse, C., Chen, M., Sigler, E., Litwin, M., Gray, S., Chess, B., Clark, J., Berner, C., McCandlish, S., Radford, A., Sutskever, I., and Amodei, D. Language models are few-shot learners, 2020. URL <https://arxiv.org/abs/2005.14165>.

Chen, L., Lu, K., Rajeswaran, A., Lee, K., Grover, A., Laskin, M., Abbeel, P., Srinivas, A., and Mordatch, I. Decision transformer: Reinforcement learning via sequence modeling, 2021. URL <https://arxiv.org/abs/2106.01345>.

Chen, Y., Wu, T., Wang, S., Feng, X., Jiang, J., McAleer, S. M., Geng, Y., Dong, H., Lu, Z., Zhu, S.-C., and Yang, Y. Towards human-level bimanual dexterous manipulation with reinforcement learning, 2022. URL <https://arxiv.org/abs/2206.08686>.

Collaboration, E., O'Neill, A., Rehman, A., Gupta, A., Madukuri, A., Gupta, A., Padalkar, A., Lee, A., Pooley, A.,

Gupta, A., Mandlekar, A., Jain, A., Tung, A., Bewley, A., Herzog, A., Irpan, A., Khazatsky, A., Rai, A., Gupta, A., Wang, A., Kolobov, A., Singh, A., Garg, A., Kembhavi, A., Xie, A., Brohan, A., Raffin, A., Sharma, A., Yavary, A., Jain, A., Balakrishna, A., Wahid, A., Burgess-Limerick, B., Kim, B., Schölkopf, B., Wulfe, B., Ichter, B., Lu, C., Xu, C., Le, C., Finn, C., Wang, C., Xu, C., Chi, C., Huang, C., Chan, C., Agia, C., Pan, C., Fu, C., Devin, C., Xu, D., Morton, D., Driess, D., Chen, D., Pathak, D., Shah, D., Büchler, D., Jayaraman, D., Kalashnikov, D., Sadigh, D., Johns, E., Foster, E., Liu, F., Ceola, F., Xia, F., Zhao, F., Frujeri, F. V., Stulp, F., Zhou, G., Sukhatme, G. S., Salhotra, G., Yan, G., Feng, G., Schiavi, G., Berseth, G., Kahn, G., Yang, G., Wang, G., Su, H., Fang, H.-S., Shi, H., Bao, H., Amor, H. B., Christensen, H. I., Furuta, H., Bharadhwaj, H., Walke, H., Fang, H., Ha, H., Mordatch, I., Radosavovic, I., Leal, I., Liang, J., Abou-Chakra, J., Kim, J., Drake, J., Peters, J., Schneider, J., Hsu, J., Vakil, J., Bohg, J., Bingham, J., Wu, J., Gao, J., Hu, J., Wu, J., Wu, J., Sun, J., Luo, J., Gu, J., Tan, J., Oh, J., Wu, J., Lu, J., Yang, J., Malik, J., Silvério, J., Hejna, J., Booher, J., Tompson, J., Yang, J., Salvador, J., Lim, J. J., Han, J., Wang, K., Rao, K., Pertsch, K., Hausman, K., Go, K., Gopalakrishnan, K., Goldberg, K., Byrne, K., Oslund, K., Kawaharazuka, K., Black, K., Lin, K., Zhang, K., Ehsani, K., Lekkala, K., Ellis, K., Rana, K., Srinivasan, K., Fang, K., Singh, K. P., Zeng, K.-H., Hatch, K., Hsu, K., Itti, L., Chen, L. Y., Pinto, L., Fei-Fei, L., Tan, L., Fan, L. J., Ott, L., Lee, L., Weihs, L., Chen, M., Lepert, M., Memmel, M., Tomizuka, M., Itkina, M., Castro, M. G., Spero, M., Du, M., Ahn, M., Yip, M. C., Zhang, M., Ding, M., Heo, M., Srirama, M. K., Sharma, M., Kim, M. J., Kanazawa, N., Hansen, N., Heess, N., Joshi, N. J., Suenderhauf, N., Liu, N., Palo, N. D., Shafullah, N. M. M., Mees, O., Kroemer, O., Bastani, O., Sanketi, P. R., Miller, P. T., Yin, P., Wohlhart, P., Xu, P., Fagan, P. D., Mitrano, P., Sermanet, P., Abbeel, P., Sundaresan, P., Chen, Q., Vuong, Q., Rafailov, R., Tian, R., Doshi, R., Mart'in-Mart'in, R., Baijal, R., Scalise, R., Hendrix, R., Lin, R., Qian, R., Zhang, R., Mendonca, R., Shah, R., Hoque, R., Julian, R., Bustamante, S., Kirmani, S., Levine, S., Lin, S., Moore, S., Bahl, S., Dass, S., Sonawani, S., Tulsiani, S., Song, S., Xu, S., Haldar, S., Karamcheti, S., Adebola, S., Guist, S., Nasiriany, S., Schaal, S., Welker, S., Tian, S., Ramamoorthy, S., Dasari, S., Belkhale, S., Park, S., Nair, S., Mirchandani, S., Osa, T., Gupta, T., Harada, T., Matsushima, T., Xiao, T., Kollar, T., Yu, T., Ding, T., Davchev, T., Zhao, T. Z., Armstrong, T., Darrell, T., Chung, T., Jain, V., Kumar, V., Vanhoucke, V., Zhan, W., Zhou, W., Burgard, W., Chen, X., Chen, X., Wang, X., Zhu, X., Geng, X., Liu, X., Liangwei, X., Li, X., Pang, Y., Lu, Y., Ma, Y. J., Kim, Y., Chebotar, Y., Zhou, Y., Zhu, Y., Wu, Y., Xu, Y., Wang, Y., Bisk, Y., Dou, Y., Cho, Y., Lee, Y., Cui, Y., Cao, Y., Wu, Y., Tang, Y., Zhu, Y., Zhang, Y., Jiang, Y., Li, Y., Li, Y., Iwasawa, Y., Matsuo, Y., Ma, Z., Xu, Z., Cui, Z. J., Zhang, Z., Fu, Z., and Lin, Z. Open x-embodiment: Robotic learning datasets and rt-x models, 2024. URL <https://arxiv.org/abs/2310.08864>.

Cui, Z. J., Pan, H., Iyer, A., Haldar, S., and Pinto, L. Dynamo: In-domain dynamics pretraining for visuo-motor control, 2024. URL <https://arxiv.org/abs/2409.12192>.

Dao, T., Fu, D. Y., Ermon, S., Rudra, A., and Ré, C. Flashattention: Fast and memory-efficient exact attention with io-awareness, 2022. URL <https://arxiv.org/abs/2205.14135>.

Dong, Q., Li, L., Dai, D., Zheng, C., Ma, J., Li, R., Xia, H., Xu, J., Wu, Z., Liu, T., Chang, B., Sun, X., Li, L., and Sui, Z. A survey on in-context learning, 2024. URL <https://arxiv.org/abs/2301.00234>.

Duan, Y., Schulman, J., Chen, X., Bartlett, P. L., Sutskever, I., and Abbeel, P. RI\$^2\$: Fast reinforcement learning via slow reinforcement learning. *CoRR*, abs/1611.02779, 2016. URL <http://arxiv.org/abs/1611.02779>.

Dulac-Arnold, G., Mankowitz, D., and Hester, T. Challenges of real-world reinforcement learning. *arXiv preprint arXiv:1904.12901*, 2019.

Elawady, A., Chhablani, G., Ramrakhy, R., Yadav, K., Batra, D., Kira, Z., and Szot, A. Relic: A recipe for 64k steps of in-context reinforcement learning for embodied ai, 2024. URL <https://arxiv.org/abs/2410.02751>.

Espeholt, L., Soyer, H., Munos, R., Simonyan, K., Mnih, V., Ward, T., Doron, Y., Firoiu, V., Harley, T., Dunning, I., Legg, S., and Kavukcuoglu, K. Impala: Scalable distributed deep-rl with importance weighted actor-learner architectures, 2018. URL <https://arxiv.org/abs/1802.01561>.

Finn, C., Abbeel, P., and Levine, S. Model-agnostic meta-learning for fast adaptation of deep networks, 2017. URL <https://arxiv.org/abs/1703.03400>.

Fu, L., Huang, H., Datta, G., Chen, L. Y., Panitch, W. C.-H., Liu, F., Li, H., and Goldberg, K. In-context imitation learning via next-token prediction, 2024. URL <https://arxiv.org/abs/2408.15980>.

Gallouédec, Q., Beeching, E., Romac, C., and Dellandréa, E. Jack of all trades, master of some, a multi-purpose transformer agent, 2024. URL <https://arxiv.org/abs/2402.09844>.

Goldie, A. D., Lu, C., Jackson, M. T., Whiteson, S., and Foerster, J. N. Can learned optimization make reinforcement learning less difficult?, 2024. URL <https://arxiv.org/abs/2407.07082>.

Grigsby, J., Fan, L., and Zhu, Y. Amago: Scalable in-context reinforcement learning for adaptive agents, 2024a. URL <https://arxiv.org/abs/2310.09971>.

Grigsby, J., Sasek, J., Parajuli, S., Adebi, D., Zhang, A., and Zhu, Y. Amago-2: Breaking the multi-task barrier in meta-reinforcement learning with transformers, 2024b. URL <https://arxiv.org/abs/2411.11188>.

Haldar, S., Peng, Z., and Pinto, L. Baku: An efficient transformer for multi-task policy learning, 2024. URL <https://arxiv.org/abs/2406.07539>.

Hein, D., Depeweg, S., Tokic, M., Udluft, S., Hentschel, A., Runkler, T. A., and Sterzing, V. A benchmark environment motivated by industrial control problems. In *2017 IEEE Symposium Series on Computational Intelligence (SSCI)*, pp. 1–8. IEEE, November 2017. doi: 10.1109/ssci.2017.8280935. URL <http://dx.doi.org/10.1109/SSCI.2017.8280935>.

Hessel, M., Soyer, H., Espeholt, L., Czarnecki, W., Schmitt, S., and van Hasselt, H. Multi-task deep reinforcement learning with popart, 2018. URL <https://arxiv.org/abs/1809.04474>.

Huang, S., Hu, J., Yang, Z., Yang, L., Luo, T., Chen, H., Sun, L., and Yang, B. Decision mamba: Reinforcement learning via hybrid selective sequence modeling, 2024. URL <https://arxiv.org/abs/2406.00079>.

Janner, M., Li, Q., and Levine, S. Offline reinforcement learning as one big sequence modeling problem, 2021. URL <https://arxiv.org/abs/2106.02039>.

Kim, M. J., Pertsch, K., Karamcheti, S., Xiao, T., Balakrishna, A., Nair, S., Rafailov, R., Foster, E., Lam, G., Sanketi, P., Vuong, Q., Kollar, T., Burchfiel, B., Tedrake, R., Sadigh, D., Levine, S., Liang, P., and Finn, C. Openvla: An open-source vision-language-action model, 2024. URL <https://arxiv.org/abs/2406.09246>.

Kirsch, L., Harrison, J., Freeman, C., Sohl-Dickstein, J., and Schmidhuber, J. Towards general-purpose in-context learning agents. In *NeurIPS 2023 Foundation Models for Decision Making Workshop*, 2023. URL <https://openreview.net/forum?id=zDTqQVGgzh>.

Kumar, A., Agarwal, R., Geng, X., Tucker, G., and Levine, S. Offline q-learning on diverse multi-task data both scales and generalizes, 2023. URL <https://arxiv.org/abs/2211.15144>.

Kurin, V., Palma, A. D., Kostrikov, I., Whiteson, S., and Kumar, M. P. In defense of the unitary scalarization for deep multi-task learning, 2023. URL <https://arxiv.org/abs/2201.04122>.

Lan, Q., Mahmood, A. R., Yan, S., and Xu, Z. Learning to optimize for reinforcement learning, 2024. URL <https://arxiv.org/abs/2302.01470>.

Laskin, M., Wang, L., Oh, J., Parisotto, E., Spencer, S., Steigerwald, R., Strouse, D., Hansen, S., Filos, A., Brooks, E., Gazeau, M., Sahni, H., Singh, S., and Mnih, V. In-context reinforcement learning with algorithm distillation, 2022. URL <https://arxiv.org/abs/2210.14215>.

Lee, J. N., Xie, A., Pacchiano, A., Chandak, Y., Finn, C., Nachum, O., and Brunskill, E. Supervised pretraining can learn in-context reinforcement learning, 2023. URL <https://arxiv.org/abs/2306.14892>.

Lee, K.-H., Nachum, O., Yang, M. S., Lee, L., Freeman, D., Guadarrama, S., Fischer, I., Xu, W., Jang, E., Michalewski, H., et al. Multi-game decision transformers. *Advances in Neural Information Processing Systems*, 35: 27921–27936, 2022.

Levine, S., Kumar, A., Tucker, G., and Fu, J. Offline reinforcement learning: Tutorial, review, and perspectives on open problems, 2020. URL <https://arxiv.org/abs/2005.01643>.

Li, K. and Malik, J. Learning to optimize, 2016. URL <https://arxiv.org/abs/1606.01885>.

Li, X. and Gong, H. Robust optimization for multilingual translation with imbalanced data, 2021. URL <https://arxiv.org/abs/2104.07639>.

Liang, J., Makoviychuk, V., Handa, A., Chentanez, N., Macklin, M., and Fox, D. Gpu-accelerated robotic simulation for distributed reinforcement learning, 2018. URL <https://arxiv.org/abs/1810.05762>.

Liu, P., Yuan, W., Fu, J., Jiang, Z., Hayashi, H., and Neubig, G. Pre-train, prompt, and predict: A systematic survey of prompting methods in natural language processing. *CoRR*, abs/2107.13586, 2021. URL <https://arxiv.org/abs/2107.13586>.

McCann, B., Keskar, N. S., Xiong, C., and Socher, R. The natural language decathlon: Multitask learning as question answering, 2018. URL <https://arxiv.org/abs/1806.08730>.

Metz, L., Maheswaranathan, N., Freeman, C. D., Poole, B., and Sohl-Dickstein, J. Tasks, stability, architecture, and compute: Training more effective learned optimizers,

and using them to train themselves, 2020. URL <https://arxiv.org/abs/2009.11243>.

Metz, L., Harrison, J., Freeman, C. D., Merchant, A., Beyer, L., Bradbury, J., Agrawal, N., Poole, B., Mordatch, I., Roberts, A., and Sohl-Dickstein, J. Velo: Training versatile learned optimizers by scaling up, 2022. URL <https://arxiv.org/abs/2211.09760>.

Min, S., Lyu, X., Holtzman, A., Artetxe, M., Lewis, M., Hajishirzi, H., and Zettlemoyer, L. Rethinking the role of demonstrations: What makes in-context learning work?, 2022. URL <https://arxiv.org/abs/2202.12837>.

Nikulin, A., Zisman, I., Zemtsov, A., Sinii, V., Kurenkov, V., and Kolesnikov, S. Xland-100b: A large-scale multi-task dataset for in-context reinforcement learning, 2024. URL <https://arxiv.org/abs/2406.08973>.

Press, O., Smith, N. A., and Lewis, M. Train short, test long: Attention with linear biases enables input length extrapolation, 2022. URL <https://arxiv.org/abs/2108.12409>.

Radford, A., Wu, J., Child, R., Luan, D., Amodei, D., Sutskever, I., et al. Language models are unsupervised multitask learners. *OpenAI blog*, 1(8):9, 2019.

Raffin, A., Hill, A., Gleave, A., Kanervisto, A., Ernestus, M., and Dormann, N. Stable-baselines3: Reliable reinforcement learning implementations. *Journal of Machine Learning Research*, 22(268):1–8, 2021. URL <http://jmlr.org/papers/v22/20-1364.html>.

Rakelly, K., Zhou, A., Quillen, D., Finn, C., and Levine, S. Efficient off-policy meta-reinforcement learning via probabilistic context variables. *CoRR*, abs/1903.08254, 2019. URL <http://arxiv.org/abs/1903.08254>.

Reed, S., Zolna, K., Parisotto, E., Colmenarejo, S. G., Novikov, A., Barth-Maron, G., Gimenez, M., Sulsky, Y., Kay, J., Springenberg, J. T., Eccles, T., Bruce, J., Razavi, A., Edwards, A., Heess, N., Chen, Y., Hadsell, R., Vinyals, O., Bordbar, M., and de Freitas, N. A generalist agent, 2022. URL <https://arxiv.org/abs/2205.06175>.

Schmidhuber, J. Reinforcement learning upside down: Don’t predict rewards—just map them to actions. *arXiv preprint arXiv:1912.02875*, 2019.

Schmied, T., Adler, T., Patil, V. P., Beck, M., Pöppel, K., Brandstetter, J., Klambauer, G., Pascanu, R., and Hochreiter, S. A large recurrent action model: xlstm enables fast inference for robotics tasks. In *NeurIPS 2024 Workshop on Open-World Agents*, 2024.

Schrittwieser, J., Antonoglou, I., Hubert, T., Simonyan, K., Sifre, L., Schmitt, S., Guez, A., Lockhart, E., Hassabis, D., Graepel, T., et al. Mastering atari, go, chess and shogi by planning with a learned model. *Nature*, 588(7839):604–609, 2020.

Schulman, J., Wolski, F., Dhariwal, P., Radford, A., and Klimov, O. Proximal policy optimization algorithms, 2017. URL <https://arxiv.org/abs/1707.06347>.

Sener, O. and Koltun, V. Multi-task learning as multi-objective optimization, 2019. URL <https://arxiv.org/abs/1810.04650>.

Shaham, U., Elbayad, M., Goswami, V., Levy, O., and Bhosale, S. Causes and cures for interference in multilingual translation, 2023. URL <https://arxiv.org/abs/2212.07530>.

Silver, D., Singh, S., Precup, D., and Sutton, R. S. Reward is enough. *Artificial Intelligence*, 299:103535, 2021.

Sinii, V., Nikulin, A., Kurenkov, V., Zisman, I., and Kolesnikov, S. In-context reinforcement learning for variable action spaces, 2024. URL <https://arxiv.org/abs/2312.13327>.

Sodhani, S., Zhang, A., and Pineau, J. Multi-task reinforcement learning with context-based representations, 2021. URL <https://arxiv.org/abs/2102.06177>.

Sridhar, K., Dutta, S., Jayaraman, D., and Lee, I. Regent: A retrieval-augmented generalist agent that can act in-context in new environments. *arXiv preprint arXiv:2412.04759*, 2024.

Sun, T., Shao, Y., Qian, H., Huang, X., and Qiu, X. Black-box tuning for language-model-as-a-service. *CoRR*, abs/2201.03514, 2022. URL <https://arxiv.org/abs/2201.03514>.

Sutton, R. S. and Barto, A. G. Reinforcement learning: An introduction. 1998.

Tarasov, D., Nikulin, A., Akimov, D., Kurenkov, V., and Kolesnikov, S. Corl: Research-oriented deep offline reinforcement learning library. *Advances in Neural Information Processing Systems*, 36, 2024.

Team, A. A., Bauer, J., Baumli, K., Baveja, S., Behbhan, F., Bhoopchand, A., Bradley-Schmieg, N., Chang, M., Clay, N., Collister, A., et al. Human-timescale adaptation in an open-ended task space. *arXiv preprint arXiv:2301.07608*, 2023.

Team, O. M., Ghosh, D., Walke, H., Pertsch, K., Black, K., Mees, O., Dasari, S., Hejna, J., Kreiman, T., Xu, C.,

Luo, J., Tan, Y. L., Chen, L. Y., Sanketi, P., Vuong, Q., Xiao, T., Sadigh, D., Finn, C., and Levine, S. Octo: An open-source generalist robot policy, 2024. URL <https://arxiv.org/abs/2405.12213>.

Todorov, E., Erez, T., and Tassa, Y. Mujoco: A physics engine for model-based control. In *2012 IEEE/RSJ International Conference on Intelligent Robots and Systems*, pp. 5026–5033, 2012. doi: 10.1109/IROS.2012.6386109.

Towers, M., Kwiatkowski, A., Terry, J., Balis, J. U., Cola, G. D., Deleu, T., Goulão, M., Kallinteris, A., Krimmel, M., KG, A., Perez-Vicente, R., Pierré, A., Schulhoff, S., Tai, J. J., Tan, H., and Younis, O. G. Gymnasium: A standard interface for reinforcement learning environments, 2024. URL <https://arxiv.org/abs/2407.17032>.

Wang, L., Chen, X., Zhao, J., and He, K. Scaling proprioceptive-visual learning with heterogeneous pre-trained transformers, 2024. URL <https://arxiv.org/abs/2409.20537>.

Wang, Z., Tsvetkov, Y., Firat, O., and Cao, Y. Gradient vaccine: Investigating and improving multi-task optimization in massively multilingual models, 2020. URL <https://arxiv.org/abs/2010.05874>.

Wulfmeier, M., Abdolmaleki, A., Hafner, R., Springenberg, J. T., Neunert, M., Hertweck, T., Lampe, T., Siegel, N., Heess, N., and Riedmiller, M. Compositional transfer in hierarchical reinforcement learning, 2020. URL <https://arxiv.org/abs/1906.11228>.

Xin, D., Ghorbani, B., Garg, A., Firat, O., and Gilmer, J. Do current multi-task optimization methods in deep learning even help?, 2022. URL <https://arxiv.org/abs/2209.11379>.

Ying, C., Hao, Z., Zhou, X., Xu, X., Su, H., Zhang, X., and Zhu, J. PEAC: Unsupervised pre-training for cross-embodiment reinforcement learning. In *The Thirty-eighth Annual Conference on Neural Information Processing Systems*, 2024. URL <https://openreview.net/forum?id=LyAFFfdx8YF>.

Yu, T., Kumar, S., Gupta, A., Levine, S., Hausman, K., and Finn, C. Gradient surgery for multi-task learning, 2020. URL <https://arxiv.org/abs/2001.06782>.

Yu, T., Quillen, D., He, Z., Julian, R., Narayan, A., Shively, H., Bellathur, A., Hausman, K., Finn, C., and Levine, S. Meta-world: A benchmark and evaluation for multi-task and meta reinforcement learning, 2021. URL <https://arxiv.org/abs/1910.10897>.

Zhang, P., Zeng, G., Wang, T., and Lu, W. Tinyllama: An open-source small language model, 2024.

Zhao, T. Z., Nagabandi, A., Rakelly, K., Finn, C., and Levine, S. MELD: meta-reinforcement learning from images via latent state models. *CoRR*, abs/2010.13957, 2020. URL <https://arxiv.org/abs/2010.13957>.

Zheng, Q., Zhang, A., and Grover, A. Online decision transformer, 2022. URL <https://arxiv.org/abs/2202.05607>.

Zhuang, Z., Peng, D., Liu, J., Zhang, Z., and Wang, D. Reinformer: Max-return sequence modeling for offline rl, 2024. URL <https://arxiv.org/abs/2405.08740>.

Zisman, I., Kurenkov, V., Nikulin, A., Sinii, V., and Kolesnikov, S. Emergence of in-context reinforcement learning from noise distillation, 2024a. URL <https://arxiv.org/abs/2312.12275>.

Zisman, I., Nikulin, A., Polubarov, A., Lyubaykin, N., and Kurenkov, V. N-gram induction heads for in-context rl: Improving stability and reducing data needs, 2024b. URL <https://arxiv.org/abs/2411.01958>.

A. Dataset Details

A.1. General Information

MuJoCo. MuJoCo (Todorov et al., 2012) is a physics engine designed for multi-joint continuous control. For our purposes, we selected 11 classic continuous control environments from OpenAI Gym (Brockman et al., 2016) and Gymnasium (Towers et al., 2024).

Meta-World. Meta-World (Yu et al., 2021) is an open-source simulated benchmark for meta-reinforcement learning and multitask learning consisting of 50 distinct robotic manipulation tasks. It is important to note that, similar to JAT (Gallouédec et al., 2024), we limit the episode length to 100 transitions to reduce dataset size and increase the number of episodes that fit within the model’s context. This truncation is feasible, as such a horizon is often sufficient to solve the task. However, this modification complicates direct performance comparisons with models such as AMAGO-2 (Grigsby et al., 2024b), which utilize full 500-step rollouts and reports total returns over three consecutive episodes.

Bi-DexHands. Bi-DexHands (Chen et al., 2022) is the first suite of bi-manual manipulation environments designed for practitioners in common RL, MARL, offline RL, multi-task RL, and Meta-RL. It provides 20 tasks that feature complex, high-dimensional continuous action and observation spaces. Some task subgroups share state and action spaces, making this benchmark applicable to the Meta-RL framework.

Industrial-Benchmark. Industrial-Benchmark (Hein et al., 2017) is a suite of synthetic continuous control problems designed to model various aspects that are crucial in industrial applications, such as the optimization and control of gas and wind turbines. The dynamic behavior of the environment, as well as its stochasticity, can be controlled through the setpoint parameter p . By varying this parameter from 0 to 100 in increments of 5, we generated 21 tasks that share a common state and action structure. Classic reward function was selected and subsequently down-scaled by a factor of 100.

A.2. Train vs. Test Tasks Split

To validate the inference-time optimization capability of our model, we divided the overall set of 102 tasks into two disjoint subsets. The validation subset was excluded from the training dataset. Below, we provide details of the split for each domain.

A.2.1. MUJOCo

Validation tasks for the MuJoCo domain were created by modifying the physical parameters of the environments using the provided XML API. For each embodiment, the default viscosity parameter was adjusted from 0 to 0.05, and 0.1. Additionally, the gravity parameter was varied by ± 10 percent.

A.2.2. META-WORLD

The standard ML45 split was selected, with 45 tasks assigned to the training set and 5 tasks reserved for validation: *bin-picking, box-close, door-lock, door-unlock, and hand-insert*.

A.2.3. BI-DEXHANDS

We adopted the ML20 benchmark setting proposed by the original authors (Chen et al., 2022), in which 15 tasks are assigned to the training set, while 5 tasks are reserved for validation, including: *door-close-outward, door-open-inward, door-open-outward, hand-kettle, and hand-over*. It is important to note that the *hand-over* task does not share the same state-action space dimensionality with any tasks in the training set, making it incompatible with the current encoder architecture. As a result, we report a performance of 0 (random) for this task.

A.2.4. INDUSTRIAL-BENCHMARK

For this domain, a global split based on the setpoint parameter was made, with setpoints ranging from 0 to 75 assigned to the training set, and setpoints from 80 to 100 assigned to the validation set.

A.3. Epsilon Decay Functions

The epsilon decay function defines how the noise proportion ϵ depends on the transition number n_s within trajectory. The primary purpose of utilizing such function is to ensure in smooth increase in the rewards through generated trajectories. A linear decay function may not yield this behavior across all environments, as some tasks exhibit rewards that increase rapidly either at the beginning or the end of trajectories when linear function is utilized. To address this variability, we employ the following generalized decay function:

$$\epsilon(n_s) = \begin{cases} \sqrt[p]{1 - (n_s / ((1 - f)N_s))^p} & n_s \leq (1 - f)N_s \\ 0 & n_s > (1 - f)N_s \end{cases}$$

where N_s represents the maximum number of transitions in a trajectory, f the fraction of the trajectory with zero noise, and p is a parameter that controls the curvature of the decay function. By adjusting p , it is possible to modulate the smoothness of the reward progression along the trajectory in order to better suit different tasks. Specifically, when rewards increase sharply at the beginning of the trajectory, setting $p > 1$ flattens the epsilon curve at the start and steepens it at the end. Conversely, when rewards increase in a sharp manner towards the end of the trajectory, choosing $0 < p < 1$ results in the epsilon curve being steepened at the start and flattened at the end.

B. Demonstrators

B.1. Training

MuJoCo. The dataset provided by JAT (Gallouédec et al., 2024) consists of demonstrations from expert RL agents on MuJoCo (Todorov et al., 2012) tasks. It was used to train demonstrators through the imitation learning paradigm. The resulting models achieve performance similar to that of the original RL agents.

Meta-World. For the Meta-World (Yu et al., 2021) benchmark, Gallouédec et al. (2024) open-sourced trained agents for each task in the benchmark. These models served as demonstrators; however, a detailed analysis revealed that certain agents exhibited suboptimal performance. Specifically, models trained on the *disassemble*, *coffee-pull*, *coffee-push*, *soccer*, *push-back*, *peg-insert-side*, and *pick-out-of-hole* tasks were either too noisy or performed unsatisfactorily. As a result, we retrained agents for these tasks.

JAT (Gallouédec et al., 2024) also provided open-source training scripts, which we utilized for hyperparameter tuning and retraining new agents. This process led to improved performance for the selected tasks. However, many demonstrators across other tasks still exhibit noisy performance.

Bi-DexHands. Demonstrators were trained using the provided PPO (Schulman et al., 2017) implementation. To enhance convergence, the number of parallel environments in IsaacGym (Liang et al., 2018) was increased from 128 to 2048. In certain environments, such as the *Re-Orientation* and *Swing-Cup* tasks, we were able to significantly surpass the expert performance reported in the original Bi-DexHands paper (Chen et al., 2022). However, even after extensive training for over 1.5 billion timesteps, some policies continued to exhibit stochastic performance.

Industrial-Benchmark. Demonstrators were trained using the PPO implementation from Stable-Baselines3 (Raffin et al., 2021). For all tasks, PPO was trained with advantage normalization, a KL-divergence limit of 0.2, 2500 environment steps, and a batch size of 50. All agents were trained for 1 million timesteps. Similarly to original Industrial Benchmark setup (Hein et al., 2017), discount factor was set to 0.97. To ensure better score comparability, we limited the episode length to 250 interactions. PPO agents were trained using both classic and delta rewards; however, we observed that agents trained on delta rewards achieved higher classic reward scores compared to those trained directly on scaled classic returns. Consequently, for our experiments, we utilize demonstrators trained with delta rewards.

C. Additional Experiments

C.1. Is Algorithm Distillation More Effective Than Expert Distillation?

To assess the benefits of AD-style training on noise-distilled trajectories over simple Expert Distillation (ED), we conducted an experiment using a model with the same architecture as Vintix—including the transformer backbone, encoders, and loss function—but trained exclusively on expert-level demonstrations. We then evaluated both the ED and AD models using the cold-start inference procedure.

Figure 8 shows that ED underperforms relative to AD in terms of asymptotic performance across both the MuJoCo and Meta-World domains. Specifically, ED converges to an average expert-normalized score of 0.8, whereas AD reaches 0.97 on MuJoCo and 0.95 on Meta-World.

These results highlight the critical role of policy-improvement structure in the dataset for enabling self-correcting behavior and achieving superior performance. Notably, while ED’s performance remains relatively stable across different shot counts in MuJoCo, it shows a positive trend in Meta-World as the number of shots increases.

C.2. Does Vintix Perform In-Context Reinforcement Learning?

To investigate whether Vintix engages in reinforcement learning during inference, we trained a variant of the model without access to reward signals. We then compared its performance to the original Vintix model (trained with rewards) using the cold-start inference procedure on training tasks from both domains.

Evaluation results (Figure 8) demonstrate that removing the reward signal significantly impairs performance. The reward-masked AD model performs worse asymptotically and exhibits slower convergence on the Meta-World domain.

These findings suggest that reward feedback is essential for effective self-improvement during inference. This supports the hypothesis that supervised training on a dataset containing policy improvement mechanisms enhances the model’s in-context reinforcement learning capabilities.

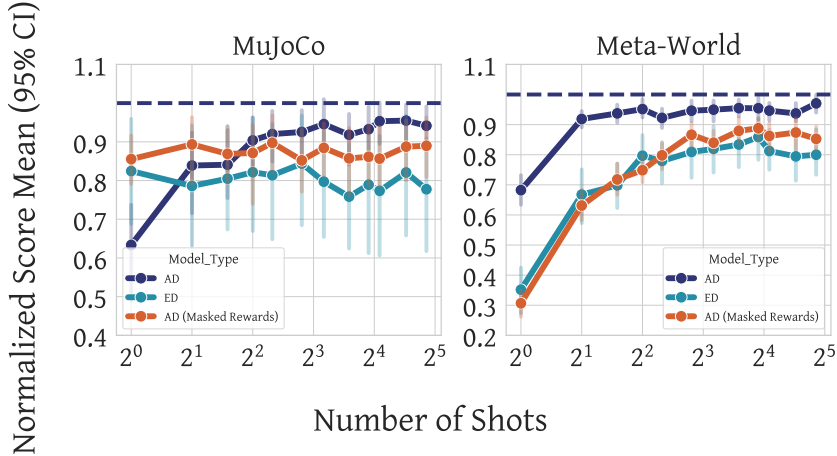


Figure 8. Performance of AD, ED and AD without rewards on MuJoCo and Meta-World domains.

D. Hyperparameters

Hyperparameter	Value
Learning Rate	0.0003
Optimizer	Adam
Beta 1	0.9
Beta 2	0.99
Batch Size	64
Gradient Accumulation Steps	2
Transformer Layers	20
Transformer Heads	16
Context Length	8192
Transformer Hidden Dim	1024
FF Hidden Size	4096
MLP Type	GptNeoxMLP
Normalization Type	LayerNorm
Training Precision	bf16
Parameters	332100768

Table 2. Hyperparameters used in training.

E. Task-Level Dataset Visualization

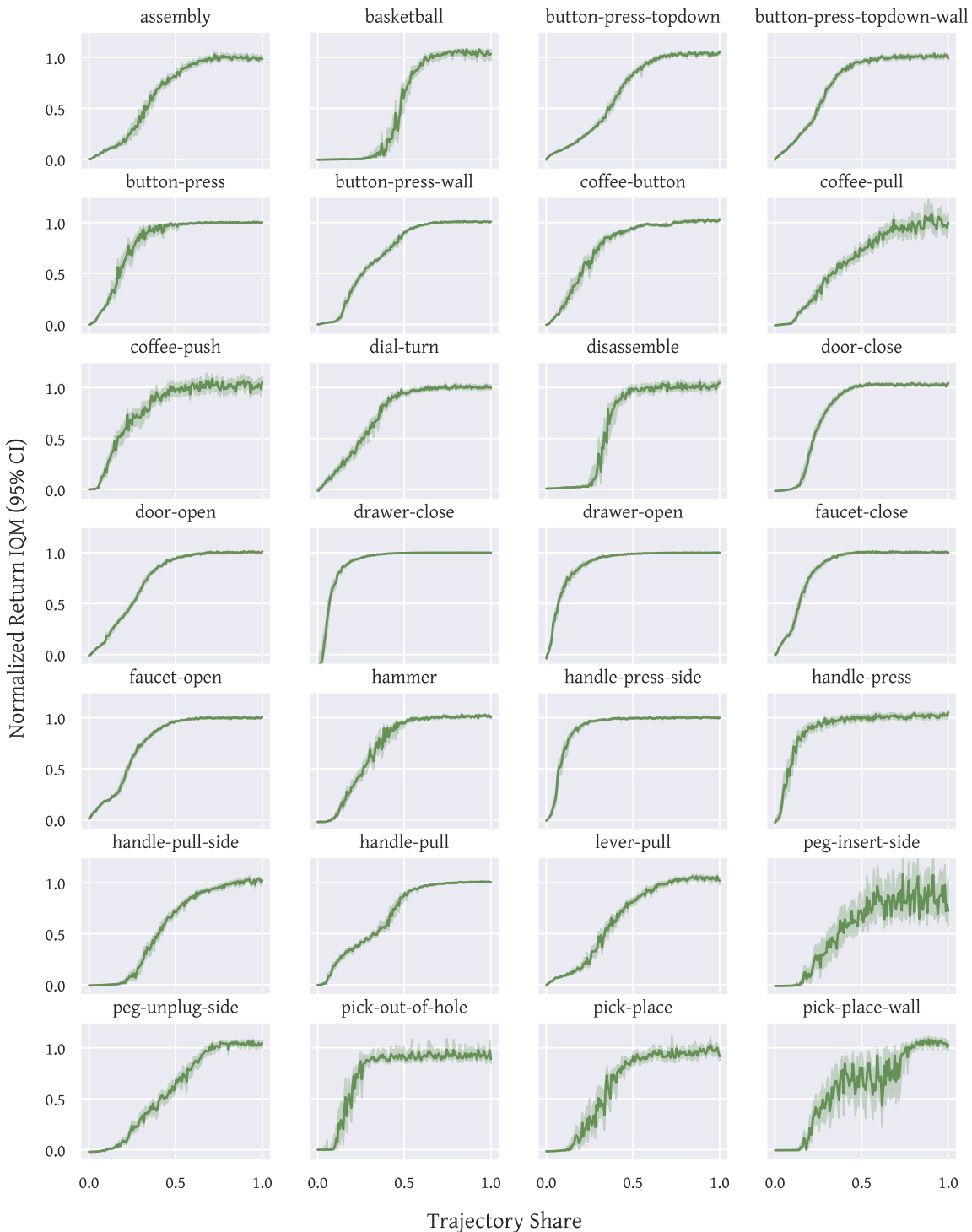


Figure 9. IQM aggregated noise-distilled trajectories for Meta-World domain (Part 1 of 2)

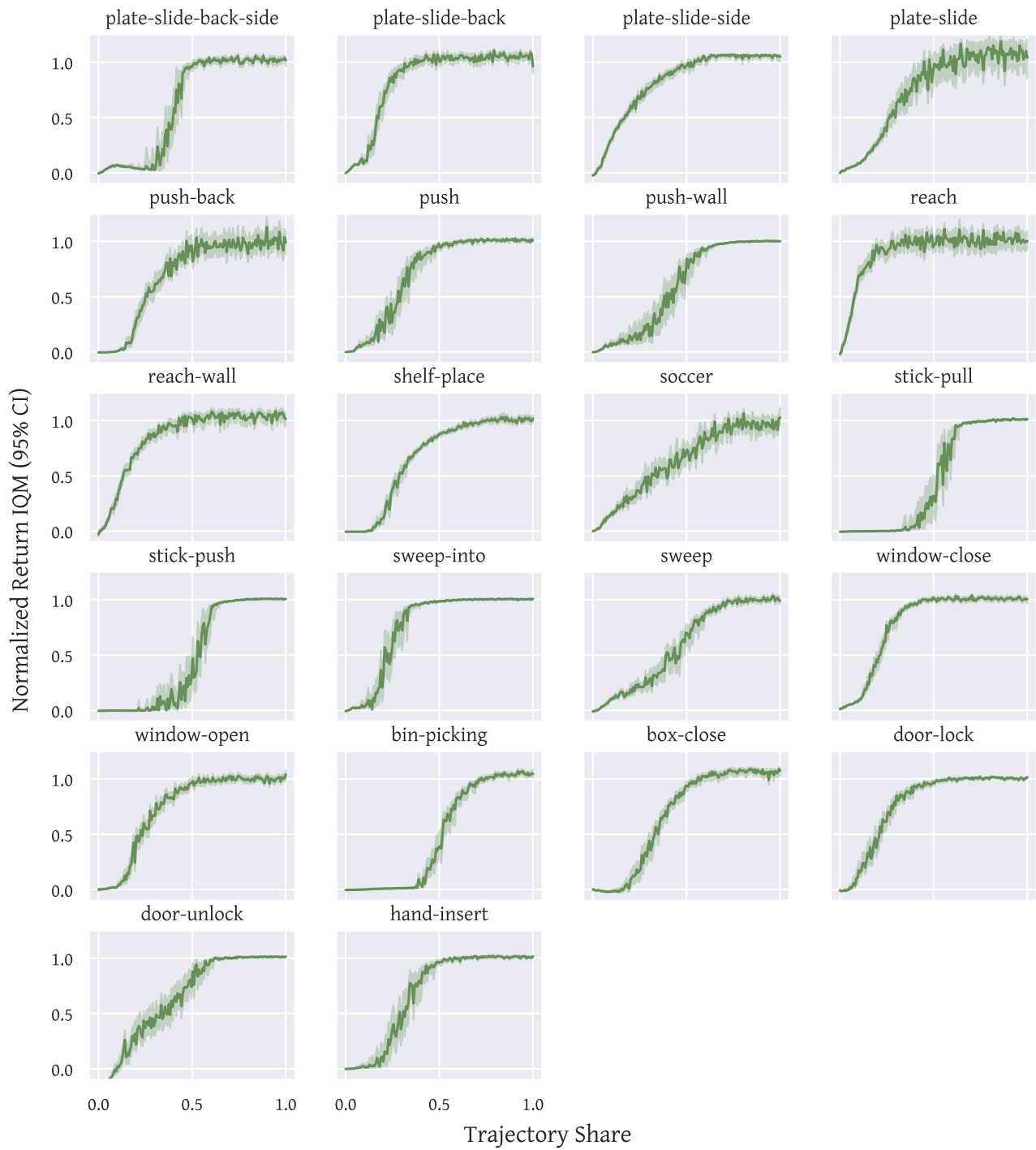


Figure 10. IQM aggregated noise-distilled trajectories for Meta-World domain (Part 2 of 2)

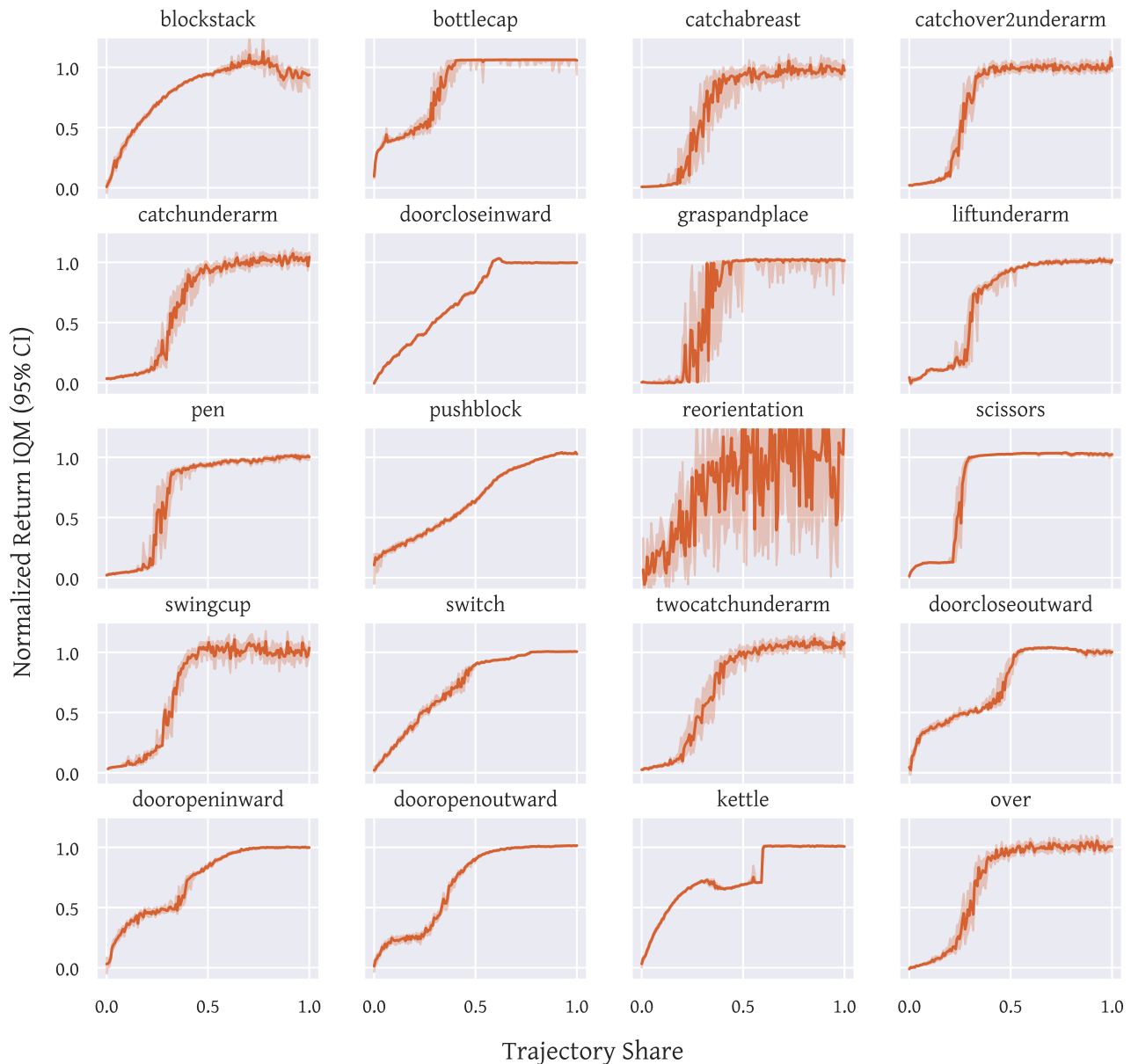


Figure 11. IQM aggregated noise-distilled trajectories for Bi-DexHands domain

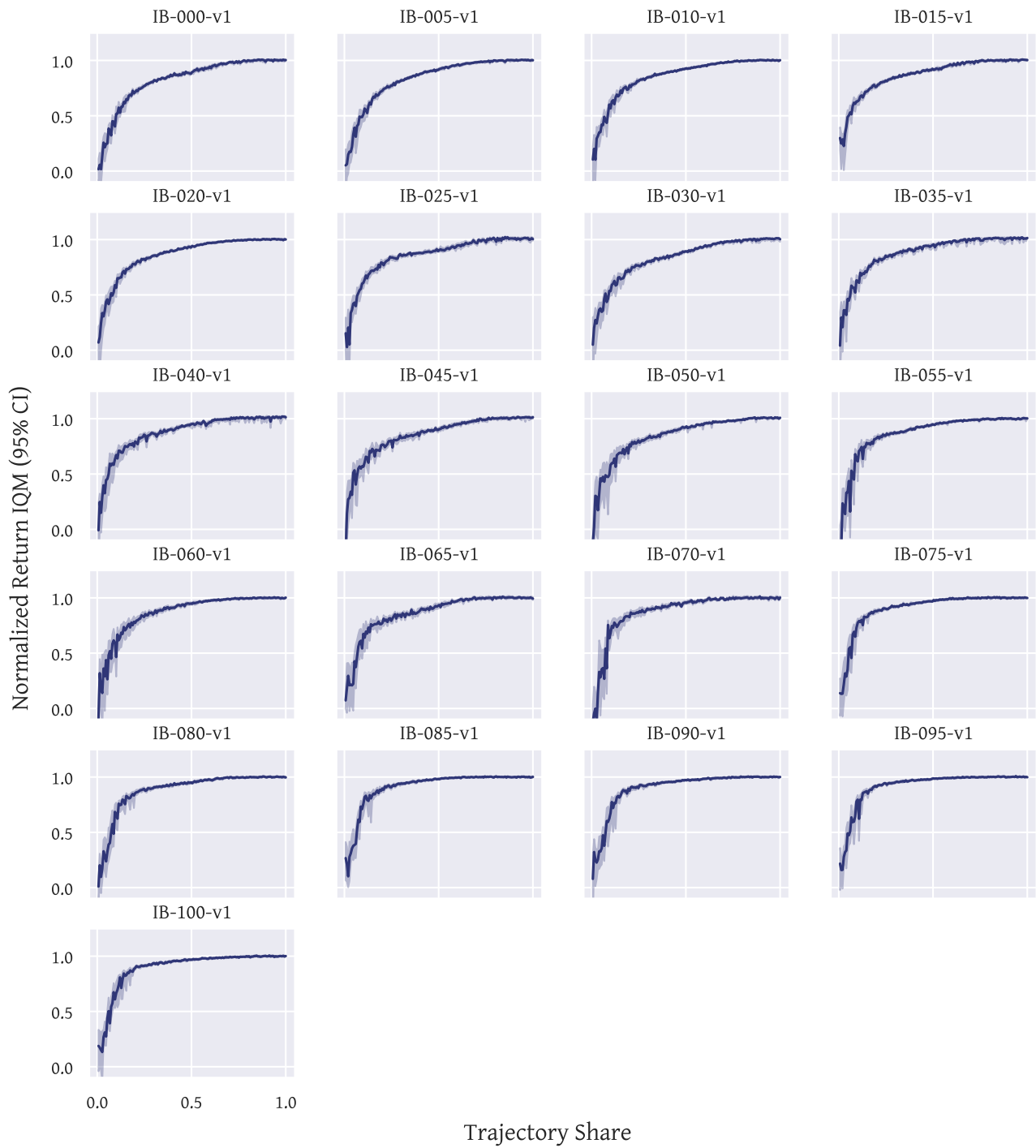


Figure 12. IQM aggregated noise-distilled trajectories for Industrial-Benchmark domain

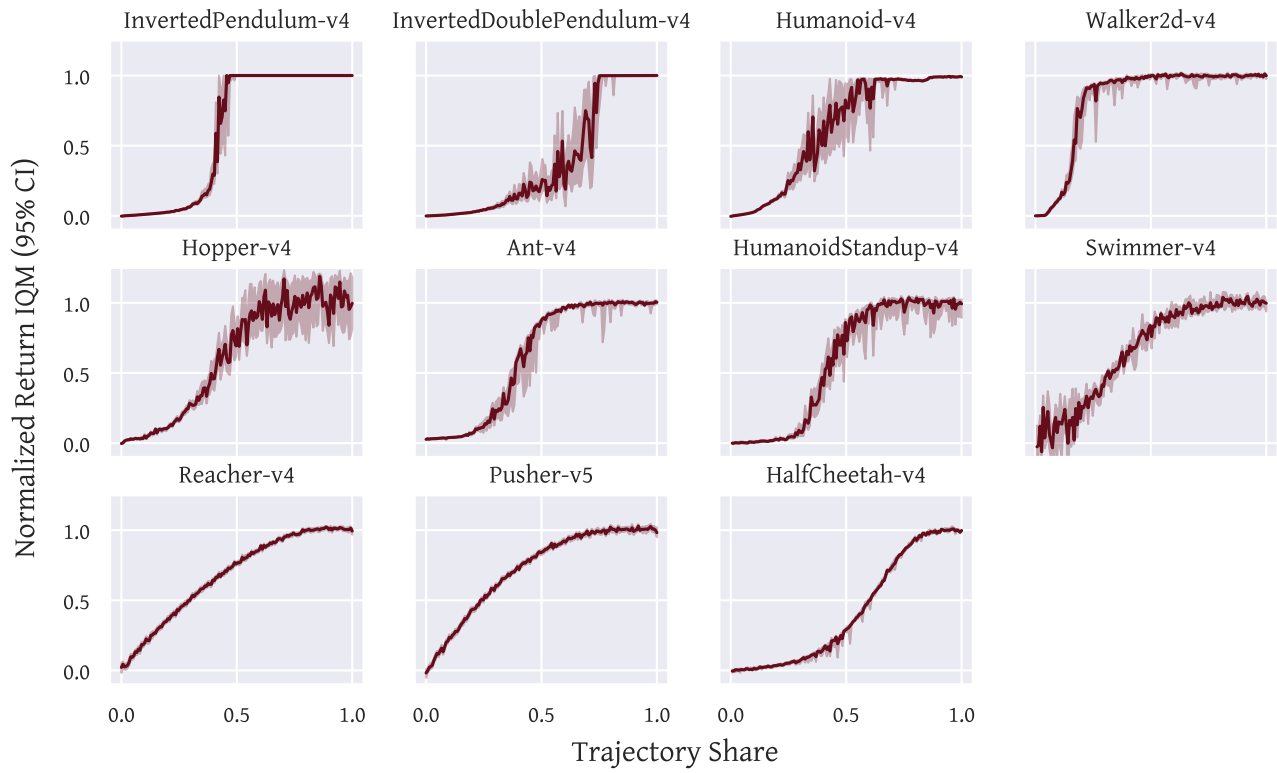


Figure 13. IQM aggregated noise-distilled trajectories for MuJoCo domain

F. Inference Time Performance Graphs

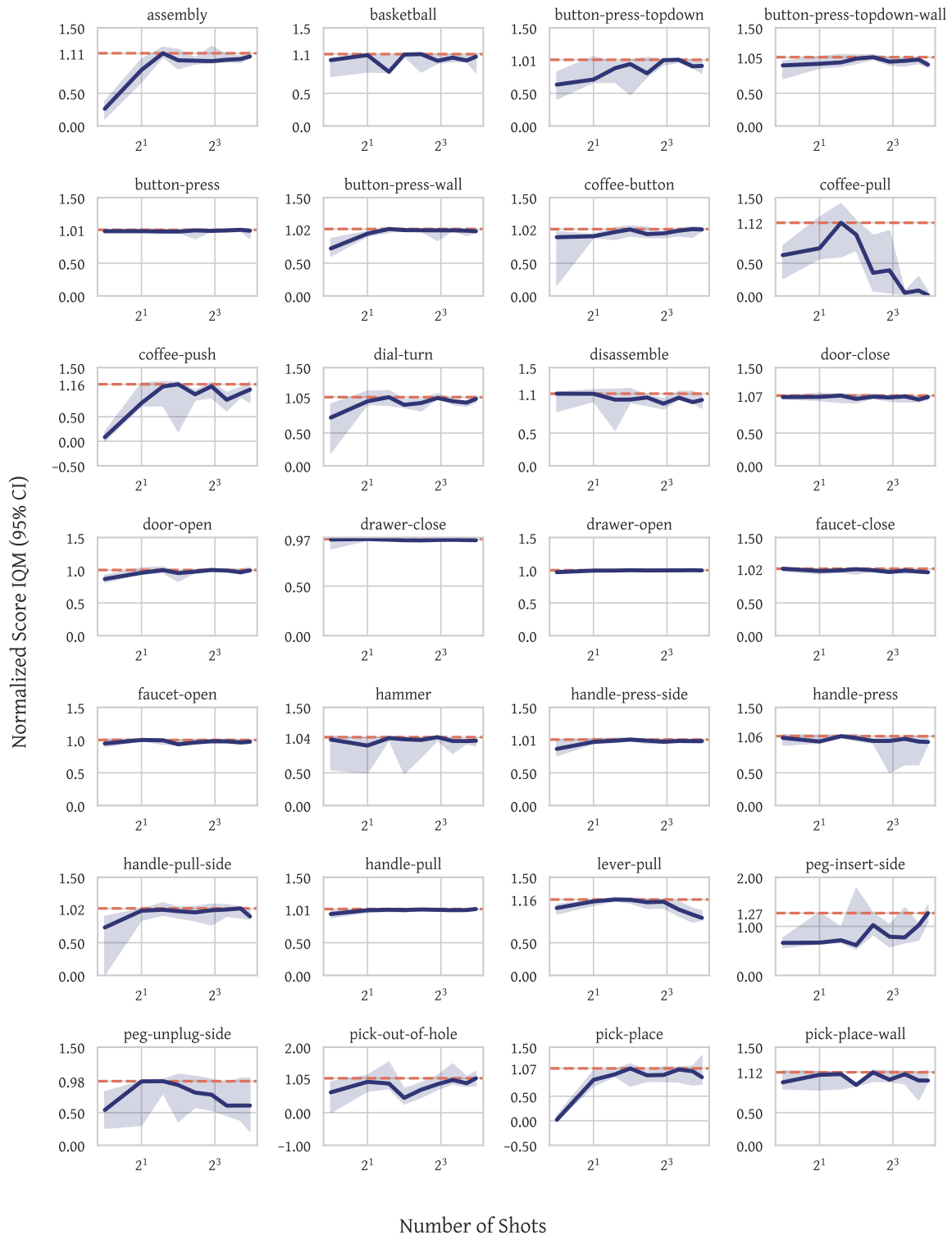


Figure 14. Inference performance for Meta-World domain (Part 1 of 2)

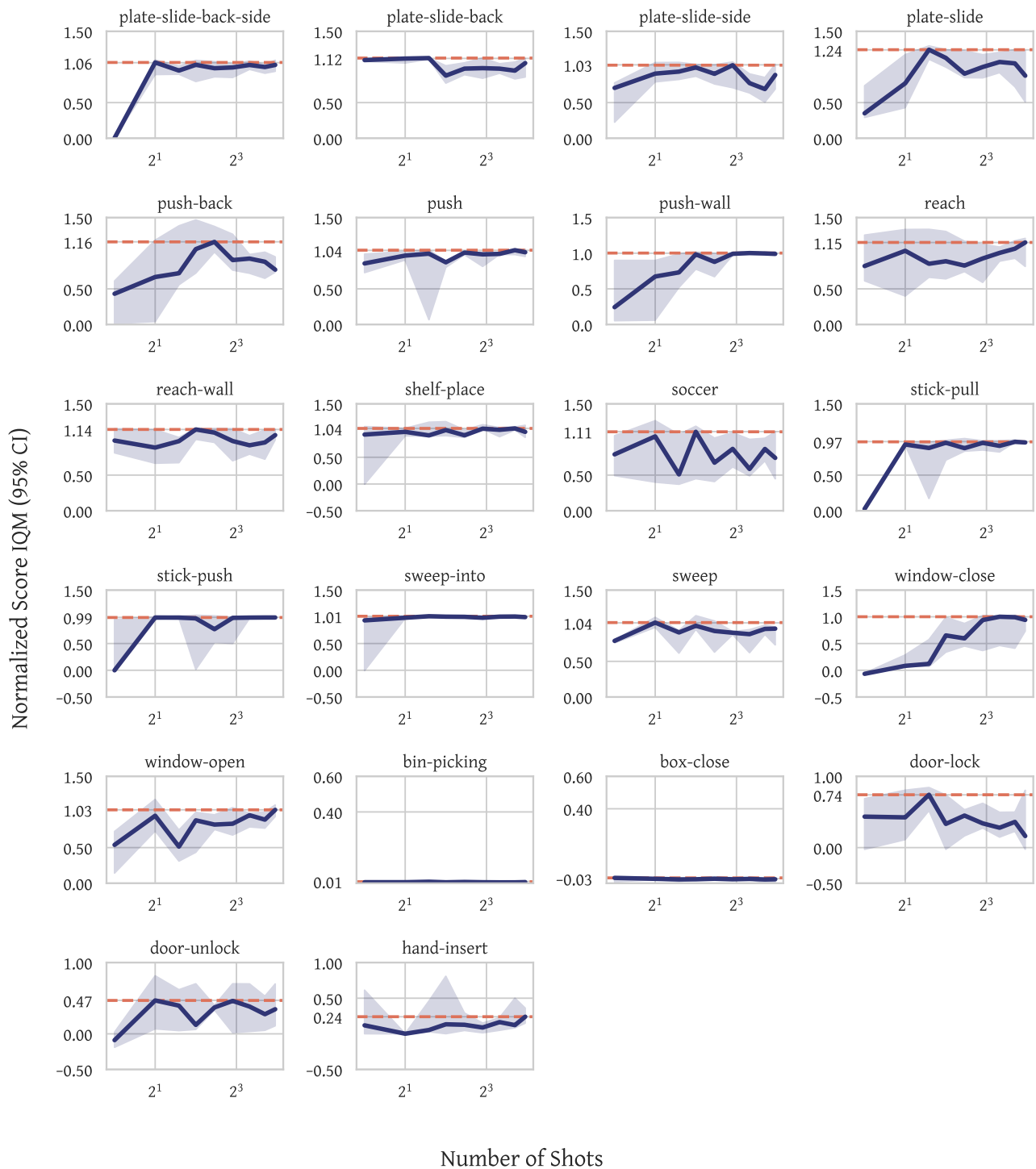


Figure 15. Inference performance for Meta-World domain (Part 2 of 2)

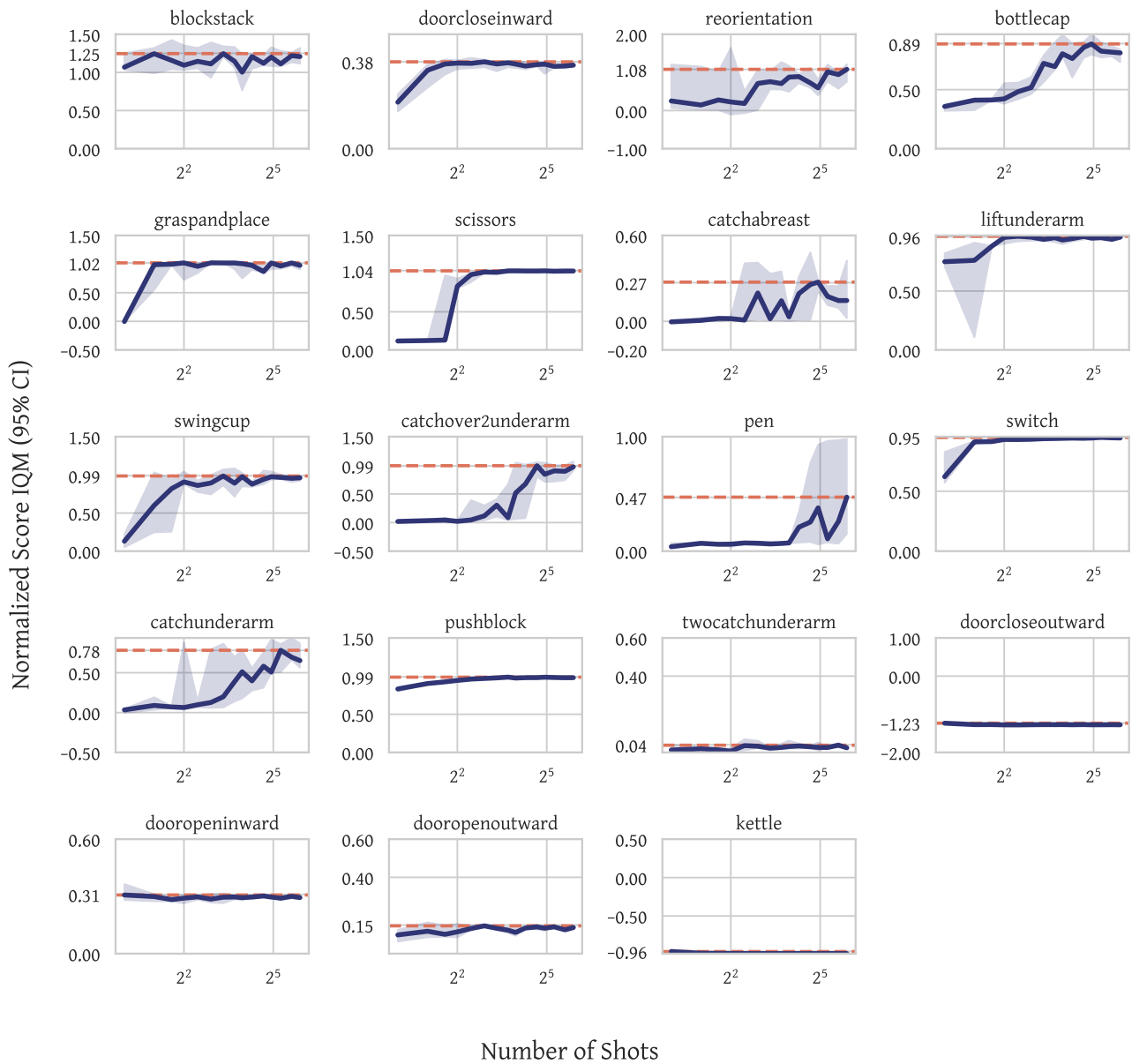


Figure 16. Inference performance for Bi-DexHands domain

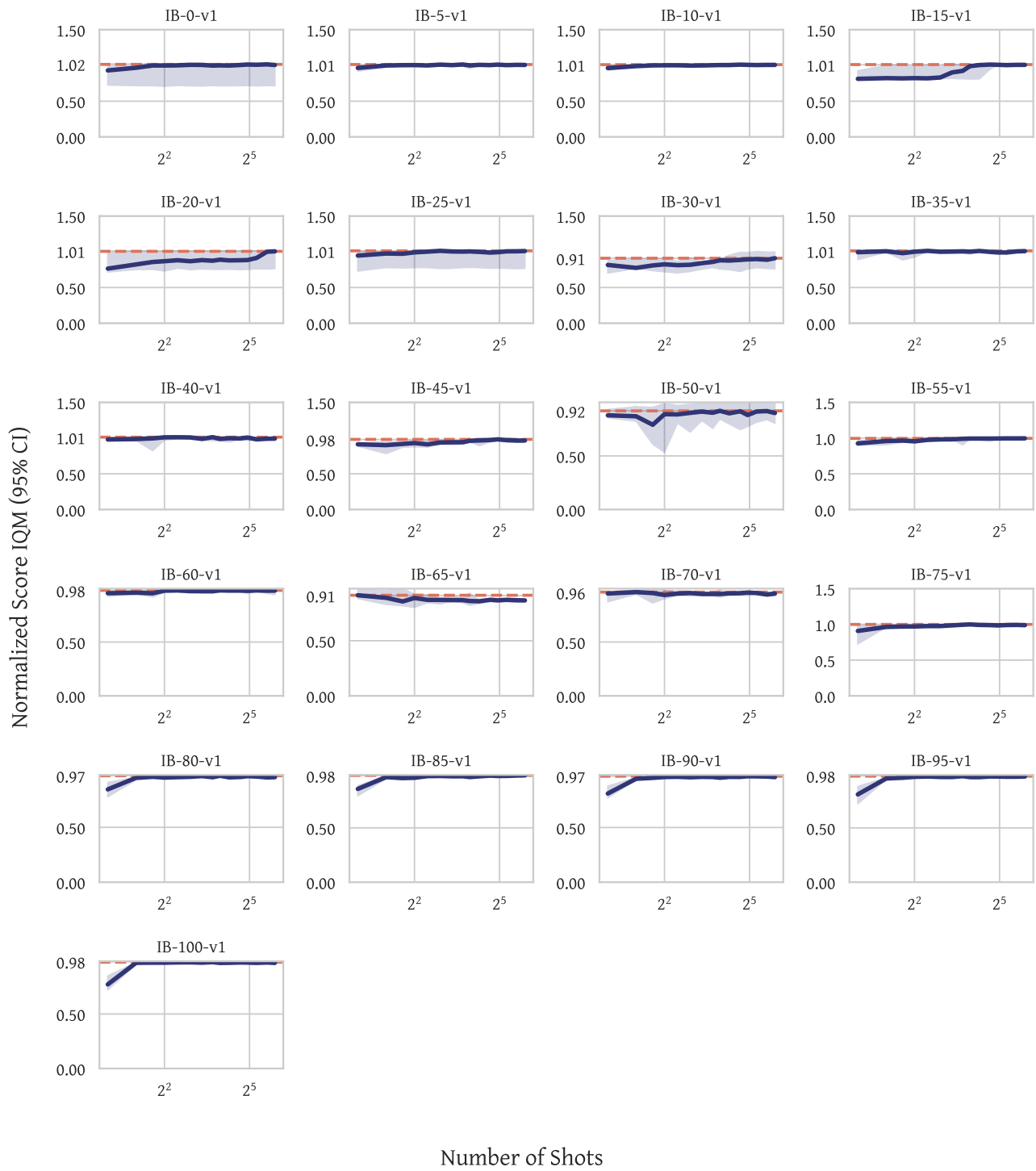


Figure 17. Inference performance for Industrial-Benchmark domain

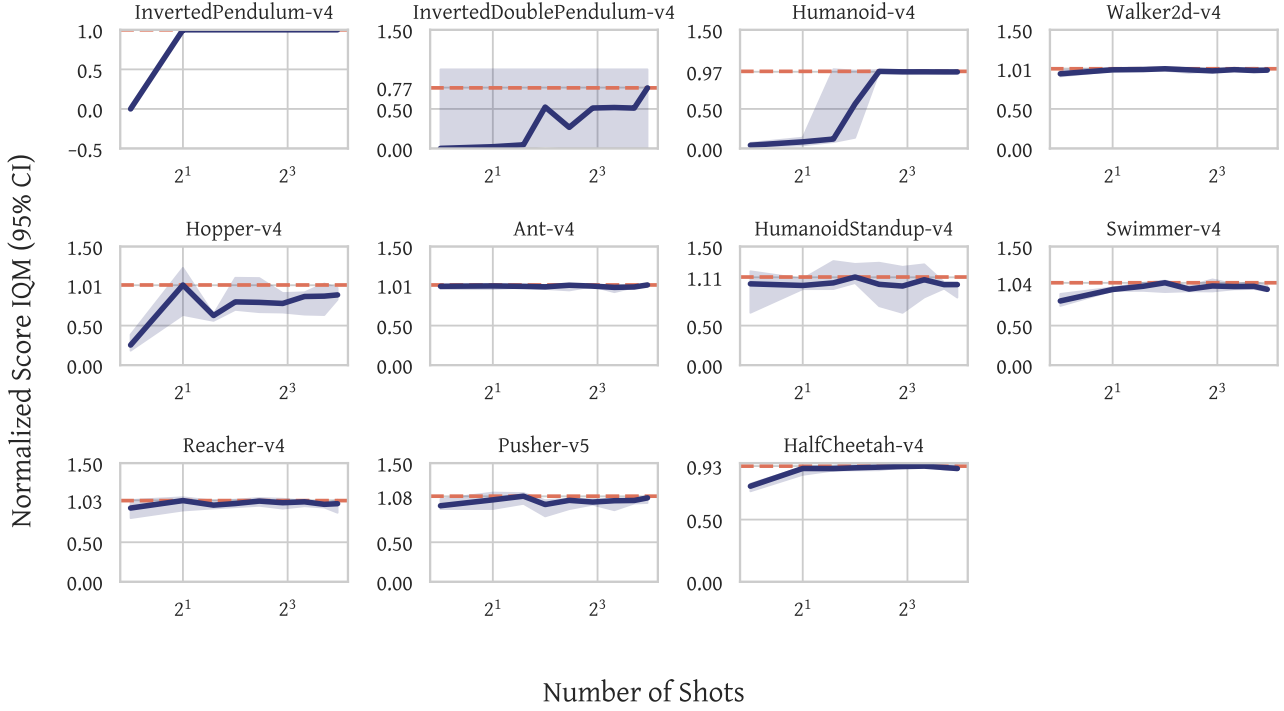


Figure 18. Inference performance for MuJoCo domain

G. Dataset Size and Metadata

Task	Trajectory Length	Number of trajectories	Mean Episode Length	State space shape	Action space shape	Reward Scaling
Hand-Block-Stack	250000	10	248.6	(428,)	(52,)	1.0
Hand-Bottle-Cap	135000	10	123.7	(420,)	(52,)	1.0
Hand-Catch-Abreast	165000	10	98.5	(422,)	(52,)	1.0
Hand-Catch-Over-2-Underarm	100000	10	55.6	(422,)	(52,)	1.0
Hand-Catch-Underarm	100000	10	64.9	(422,)	(52,)	1.0
Hand-Door-Close-Inward	100000	10	23.8	(417,)	(52,)	1.0
Hand-Grasp-And-Place	500000	8	332.6	(425,)	(52,)	1.0
Hand-Lift-Underarm	500000	10	455.0	(417,)	(52,)	1.0
Hand-Pen	135000	10	120.5	(417,)	(52,)	1.0
Hand-Push-Block	135000	10	123.2	(428,)	(52,)	1.0
Hand-Reorientation	600000	7	463.9	(422,)	(40,)	1.0
Hand-Scissors	175000	10	149.0	(417,)	(52,)	1.0
Hand-Swing-Cup	320000	10	299.0	(417,)	(52,)	1.0
Hand-Switch	135000	10	124.0	(417,)	(52,)	1.0
Hand-Two-Catch-Underarm	100000	10	65.1	(446,)	(52,)	1.0
Hand-Door-Close-Outward	265000	10	249.0	(417,)	(52,)	1.0
Hand-Door-Open-Inward	265000	10	249.0	(417,)	(52,)	1.0
Hand-Door-Open-Outward	250000	10	249.0	(417,)	(52,)	1.0
Hand-Kettle	135000	10	124.0	(417,)	(52,)	1.0
Hand-Over	100000	10	64.4	(398,)	(40,)	1.0

Table 4. Bi-DexHands - Detailed information about collected dataset

Task	Trajectory Length	Number of trajectories	Mean Episode Length	State space shape	Action space shape	Reward Scaling
assembly	100000	15	100	(39,)	(4,)	1.0
basketball	100000	15	100	(39,)	(4,)	1.0
bin-picking	100000	5	100	(39,)	(4,)	1.0
box-close	100000	5	100	(39,)	(4,)	1.0
button-press	100000	15	100	(39,)	(4,)	1.0
button-press-topdown	100000	15	100	(39,)	(4,)	1.0
button-press-topdown-wall	100000	15	100	(39,)	(4,)	1.0
button-press-wall	100000	15	100	(39,)	(4,)	1.0
coffee-button	100000	15	100	(39,)	(4,)	1.0
coffee-pull	100000	15	100	(39,)	(4,)	1.0
coffee-push	100000	15	100	(39,)	(4,)	1.0
dial-turn	100000	15	100	(39,)	(4,)	1.0
disassemble	100000	15	100	(39,)	(4,)	1.0
door-close	100000	15	100	(39,)	(4,)	1.0
door-lock	100000	5	100	(39,)	(4,)	1.0
door-open	100000	15	100	(39,)	(4,)	1.0
door-unlock	100000	5	100	(39,)	(4,)	1.0
drawer-close	100000	15	100	(39,)	(4,)	1.0
drawer-open	100000	15	100	(39,)	(4,)	1.0
faucet-close	100000	15	100	(39,)	(4,)	1.0
faucet-open	100000	15	100	(39,)	(4,)	1.0
hammer	100000	15	100	(39,)	(4,)	1.0
hand-insert	100000	5	100	(39,)	(4,)	1.0
handle-press	100000	15	100	(39,)	(4,)	1.0
handle-press-side	100000	15	100	(39,)	(4,)	1.0
handle-pull	100000	15	100	(39,)	(4,)	1.0
handle-pull-side	100000	15	100	(39,)	(4,)	1.0
lever-pull	100000	15	100	(39,)	(4,)	1.0
peg-insert-side	100000	15	100	(39,)	(4,)	1.0
peg-unplug-side	100000	15	100	(39,)	(4,)	1.0
pick-out-of-hole	100000	15	100	(39,)	(4,)	1.0
pick-place	100000	15	100	(39,)	(4,)	1.0
pick-place-wall	100000	15	100	(39,)	(4,)	1.0
plate-slide	100000	15	100	(39,)	(4,)	1.0
plate-slide-back	100000	15	100	(39,)	(4,)	1.0
plate-slide-back-side	100000	15	100	(39,)	(4,)	1.0
plate-slide-side	100000	15	100	(39,)	(4,)	1.0
push	100000	15	100	(39,)	(4,)	1.0
push-back	100000	15	100	(39,)	(4,)	1.0
push-wall	100000	15	100	(39,)	(4,)	1.0
reach	100000	15	100	(39,)	(4,)	1.0
reach-wall	100000	15	100	(39,)	(4,)	1.0
shelf-place	100000	15	100	(39,)	(4,)	1.0
soccer	100000	15	100	(39,)	(4,)	1.0
stick-pull	100000	15	100	(39,)	(4,)	1.0
stick-push	100000	15	100	(39,)	(4,)	1.0
sweep	100000	15	100	(39,)	(4,)	1.0
sweep-into	100000	15	100	(39,)	(4,)	1.0
window-close	100000	15	100	(39,)	(4,)	1.0
window-open	100000	15	100	(39,)	(4,)	1.0

Table 3. Meta-World - Detailed information about collected dataset

Task	Trajectory Length	Number of trajectories	Mean Episode Length	State space shape	Action space shape	Reward Scaling
Ant-v4	1000000	10	524.1	(105,)	(8,)	0.1
HalfCheetah-v4	1000000	5	1000	(17,)	(6,)	0.1
Hopper-v4	1000000	10	227.3	(11,)	(3,)	0.1
Humanoid-v4	1000000	15	207.7	(348,)	(17,)	0.1
HumanoidStandup-v4	1000000	15	1000	(348,)	(17,)	0.01
InvertedDoublePendulum-v4	1000000	10	55.7	(9,)	(1,)	0.1
InvertedPendulum-v4	1000000	10	68.2	(4,)	(1,)	0.1
Pusher-v5	1000000	5	100	(23,)	(7,)	0.1
Reacher-v4	1000000	5	50	(10,)	(2,)	0.1
Swimmer-v4	1000000	5	1000	(8,)	(2,)	1.0
Walker2d-v4	1000000	10	350.2	(17,)	(6,)	0.1

Table 5. MuJoCo - Detailed information about collected dataset

Task	Trajectory Length	Number of trajectories	Mean Episode Length	State space shape	Action space shape	Reward Scaling
IB-p-0	100000	15	250	(6,)	(3,)	1.0
IB-p-5	100000	15	250	(6,)	(3,)	1.0
IB-p-10	100000	15	250	(6,)	(3,)	1.0
IB-p-15	100000	15	250	(6,)	(3,)	1.0
IB-p-20	100000	15	250	(6,)	(3,)	1.0
IB-p-25	100000	15	250	(6,)	(3,)	1.0
IB-p-30	100000	15	250	(6,)	(3,)	1.0
IB-p-35	100000	15	250	(6,)	(3,)	1.0
IB-p-40	100000	15	250	(6,)	(3,)	1.0
IB-p-45	100000	15	250	(6,)	(3,)	1.0
IB-p-50	100000	15	250	(6,)	(3,)	1.0
IB-p-55	100000	15	250	(6,)	(3,)	1.0
IB-p-60	100000	15	250	(6,)	(3,)	1.0
IB-p-65	100000	15	250	(6,)	(3,)	1.0
IB-p-70	100000	15	250	(6,)	(3,)	1.0
IB-p-75	100000	15	250	(6,)	(3,)	1.0
IB-p-80	100000	15	250	(6,)	(3,)	1.0
IB-p-85	100000	15	250	(6,)	(3,)	1.0
IB-p-90	100000	15	250	(6,)	(3,)	1.0
IB-p-95	100000	15	250	(6,)	(3,)	1.0
IB-p-100	100000	15	250	(6,)	(3,)	1.0

Table 6. Industrial-Benchmark - Detailed information about collected dataset

H. Task-Level Performance

Task	Random Score	Expert Score	Vintix (Normalized)
assembly	45,1 ± 3,3	297,9 ± 24,8	1.04 ± 0.10
basketball	3 ± 1,3	558,4 ± 69,3	1.02 ± 0.11
bin-picking	2 ± 0,6	424 ± 105,7	0.01 ± 0.01
box-close	78,7 ± 11,6	520 ± 122,6	-0.04 ± 0.03
button-press	31,3 ± 4,3	642,9 ± 13	0.97 ± 0.07
button-press-topdown	31,6 ± 9,8	483,7 ± 41,7	0.94 ± 0.14
button-press-topdown-wall	30,8 ± 9	497,9 ± 31,2	0.97 ± 0.07
button-press-wall	10,3 ± 4,4	675,9 ± 15,2	1.00 ± 0.04
coffee-button	33,1 ± 7,8	731,4 ± 29,1	1.00 ± 0.06
coffee-pull	4,3 ± 0,5	294 ± 103,6	0.07 ± 0.20
coffee-push	4,3 ± 0,7	564,8 ± 106,7	1.01 ± 0.20
dial-turn	35,8 ± 42,8	788,4 ± 82,4	0.99 ± 0.07
disassemble	40,6 ± 6,8	527,3 ± 64,6	1.00 ± 0.12
door-close	5,5 ± 1,4	541,9 ± 25,6	1.02 ± 0.05
door-lock	115,7 ± 30,1	805,5 ± 42,7	0.35 ± 0.36
door-open	58,9 ± 10,1	587,6 ± 18,4	0.99 ± 0.05
door-unlock	99,8 ± 17,8	803,1 ± 19,6	0.21 ± 0.26
drawer-close	147,4 ± 291,1	868,4 ± 3,3	0.96 ± 0.01
drawer-open	126,3 ± 23,3	492,9 ± 2,5	1.00 ± 0.01
faucet-close	260,9 ± 26,4	755,4 ± 20,8	0.99 ± 0.03
faucet-open	242,7 ± 24,5	746,9 ± 12,9	0.97 ± 0.03
hammer	93,9 ± 9,7	687,6 ± 49,9	0.97 ± 0.12
hand-insert	2,7 ± 0,8	738,2 ± 36,6	0.19 ± 0.20
handle-press	73,6 ± 76,1	812,8 ± 170,8	1.00 ± 0.15
handle-press-side	59,4 ± 26,8	860,3 ± 32,8	0.99 ± 0.02
handle-pull	9,5 ± 6,5	703,3 ± 15,2	1.00 ± 0.02
handle-pull-side	2,1 ± 0,5	495,3 ± 49,3	1.00 ± 0.11
lever-pull	66,9 ± 16,9	575,5 ± 67,9	0.96 ± 0.16
peg-insert-side	1,8 ± 0,3	330,1 ± 159,4	1.01 ± 0.40
peg-unplug-side	4,6 ± 2,5	528,8 ± 87,1	0.75 ± 0.34
pick-out-of-hole	8,6 ± 49,9	401,1 ± 105,8	0.91 ± 0.20
pick-place	1,5 ± 0,9	423,6 ± 97,5	0.98 ± 0.22
pick-place-wall	0 ± 0	515,4 ± 162,5	1.04 ± 0.16
plate-slide	76,5 ± 12	531,1 ± 152	0.99 ± 0.34
plate-slide-back	33,8 ± 9,5	719,5 ± 88	0.99 ± 0.16
plate-slide-back-side	35,9 ± 13	727,5 ± 69,5	0.99 ± 0.09
plate-slide-side	22,6 ± 14	693,6 ± 82,4	0.83 ± 0.22
push	5,8 ± 2,6	747,7 ± 61,5	0.97 ± 0.14
push-back	1,2 ± 0,1	396,2 ± 109,3	0.95 ± 0.29
push-wall	6,5 ± 4	749,7 ± 11,7	0.99 ± 0.02
reach	154 ± 52,8	679,6 ± 131,8	1.01 ± 0.26
reach-wall	149 ± 35,7	748,2 ± 102,1	0.98 ± 0.17
shelf-place	0 ± 0	266,5 ± 30	1.01 ± 0.11
soccer	5,3 ± 3,9	509,3 ± 136,1	0.80 ± 0.35
stick-pull	2,8 ± 1,4	529,2 ± 20,9	0.92 ± 0.16
stick-push	2,9 ± 1,1	626 ± 46,9	0.90 ± 0.28
sweep	12,4 ± 8,5	518,4 ± 48	0.94 ± 0.12
sweep-into	16,9 ± 14,3	799 ± 14,9	1.00 ± 0.02
window-close	58,2 ± 15	591,1 ± 38,6	0.95 ± 0.17
window-open	42,9 ± 7,6	594,9 ± 56,2	0.96 ± 0.17

Table 7. Random, expert, and Vintix scores for Meta-World domain. Note that, here, we reported scores as in comparison to JAT model.

Task	Random Score	Expert Score	Vintix (Normalized)
Ant-v4	-459,2 ± 824,1	6368,2 ± 593,8	0,98 ± 0,10
HalfCheetah-v4	-299,8 ± 74,4	7782,8 ± 109,2	0,93 ± 0,03
Hopper-v4	16,2 ± 8,4	3237,8 ± 707,8	0,86 ± 0,19
Humanoid-v4	116,5 ± 31,6	7527,5 ± 38,8	0,97 ± 0,00
HumanoidStandup-v4	37285,5 ± 3178	300990,1 ± 47970,1	1,02 ± 0,21
InvertedDoublePendulum-v4	56,2 ± 16,1	9332,4 ± 498,1	0,65 ± 0,47
InvertedPendulum-v4	5,6 ± 2,1	1000 ± 0	1,00 ± 0,00
Pusher-v5	-151,9 ± 8	-40,1 ± 7	1,02 ± 0,08
Reacher-v4	-41,7 ± 3,4	-5,6 ± 2,6	0,98 ± 0,07
Swimmer-v4	3 ± 11,2	95,5 ± 3,6	0,98 ± 0,06
Walker2d-v4	3,4 ± 6,4	5349,7 ± 254,6	1,00 ± 0,02

Table 8. Random, expert, and Vintix scores for the MuJoCo domain. Note that, here, we reported scores as in comparison to JAT model.

Task	Random Score	Expert Score	Vintix (Normalized)
shadowhandblockstack	95,6 ± 16	285 ± 41,8	1,17 ± 0,23
shadowhandbottlecap	110,6 ± 17,6	399,9 ± 57,6	0,81 ± 0,25
shadowhandcatchabreast	1,1 ± 0,6	65,6 ± 14,2	0,17 ± 0,32
shadowhandcatchover2underarm	4,9 ± 0,7	34,2 ± 6,1	0,92 ± 0,24
shadowhandcatchunderarm	1,7 ± 0,6	25,1 ± 6,1	0,72 ± 0,39
shadowhanddoorcloseinward	1,2 ± 0,5	8,8 ± 0,2	0,36 ± 0,02
shadowhanddoorcloseoutward	941,2 ± 43,8	1377,5 ± 15,7	-1,27 ± 0,01
shadowhanddooropeninward	-4,4 ± 41,3	409,9 ± 3,2	0,29 ± 0,02
shadowhanddooropenoutward	20,4 ± 40,9	617,1 ± 4,4	0,13 ± 0,02
shadowhandgraspandplace	6,8 ± 1,6	498,1 ± 51,1	0,97 ± 0,18
shadowhandkettle	-191,9 ± 14,8	54,5 ± 4,2	-0,99 ± 0,00
shadowhandliftunderarm	-42,7 ± 8,4	404 ± 10,1	0,95 ± 0,03
shadowhandover	2,7 ± 0,7	34,6 ± 5,8	0,95 ± 0,03
shadowhandpen	4,5 ± 2,4	186,3 ± 19,5	0,52 ± 0,44
shadowhandpushblock	224,7 ± 66,5	457,4 ± 3,6	0,98 ± 0,01
shadowhandreorientation	127,1 ± 434,9	3040,1 ± 1986,8	0,89 ± 0,66
shadowhandscissors	-23,3 ± 16,8	735,6 ± 24,8	1,03 ± 0,01
shadowhandswingcup	-414,1 ± 27,9	3937,9 ± 601,1	0,95 ± 0,13
shadowhandswitch	50,4 ± 12,5	281,3 ± 1,1	0,95 ± 0,01
shadowhandtwocatchunderarm	2,2 ± 1,1	24,8 ± 6	0,03 ± 0,03

Table 9. Random and expert scores for Bi-DexHands domain

Task	Random Score	Expert Score	Vintix (Normalized)
industrial-benchmark-0-v1	-348,9 ± 32,7	-180,7 ± 3,1	0.94 ± 0.13
industrial-benchmark-5-v1	-379,7 ± 59	-193,8 ± 2,3	1.00 ± 0.02
industrial-benchmark-10-v1	-395,4 ± 68,9	-215,1 ± 2	1.01 ± 0.01
industrial-benchmark-15-v1	-424,4 ± 83	-229,8 ± 4	1.01 ± 0.02
industrial-benchmark-20-v1	-455,8 ± 88,2	-249,4 ± 2,2	0.95 ± 0.11
industrial-benchmark-25-v1	-453,6 ± 78,8	-272,4 ± 5,5	0.95 ± 0.11
industrial-benchmark-30-v1	-480,3 ± 76,6	-288,3 ± 5,4	0.90 ± 0.10
industrial-benchmark-35-v1	-508,5 ± 87	-314,1 ± 6,7	1.00 ± 0.03
industrial-benchmark-40-v1	-515,8 ± 77,4	-337,8 ± 8,8	0.99 ± 0.05
industrial-benchmark-45-v1	-543,3 ± 85,1	-360,9 ± 7,4	0.97 ± 0.04
industrial-benchmark-50-v1	-574,9 ± 69,8	-377,9 ± 7	0.91 ± 0.09
industrial-benchmark-55-v1	-597,6 ± 69,9	-402,1 ± 6	0.99 ± 0.01
industrial-benchmark-60-v1	-625,2 ± 83,4	-430,3 ± 4,8	0.98 ± 0.02
industrial-benchmark-65-v1	-649,6 ± 62,2	-449,8 ± 4,1	0.86 ± 0.04
industrial-benchmark-70-v1	-691,7 ± 87	-471,1 ± 4,2	0.95 ± 0.03
industrial-benchmark-75-v1	-717,2 ± 72,3	-474,3 ± 3,2	0.99 ± 0.01
industrial-benchmark-80-v1	-757,8 ± 105,9	-485,4 ± 3,1	0.96 ± 0.01
industrial-benchmark-85-v1	-812,8 ± 154,9	-507,6 ± 2,9	0.98 ± 0.01
industrial-benchmark-90-v1	-846,4 ± 132,7	-522 ± 3,6	0.97 ± 0.01
industrial-benchmark-95-v1	-895,5 ± 146,5	-545,8 ± 3,3	0.97 ± 0.01
industrial-benchmark-100-v1	-986 ± 199	-561,8 ± 4,6	0.97 ± 0.01

Table 10. Random and expert scores for Industrial Benchmark domain

I. Comparison with other cross-domain agents

Task	Vintix	REGENT	JAT (Full Dataset)
Ant	0.98 ± 0.10	0.17	0.88 ± 0.29
HalfCheetah	0.93 ± 0.03	0.34	0.89 ± 0.03
Hopper	0.86 ± 0.19	0.12	0.76 ± 0.21
Humanoid	0.97 ± 0.00	0.02	0.10 ± 0.02
HumanoidStandup	1.02 ± 0.21	0.26	0.35 ± 0.09
InvertedDoublePendulum	0.65 ± 0.47	0.02	0.93 ± 0.14
InvertedPendulum	1.00 ± 0.00	0.06	0.24 ± 0.05
Pusher	1.02 ± 0.08	0.90	1.00 ± 0.05
Reacher	0.98 ± 0.07	0.90	0.99 ± 0.06
Swimmer	0.98 ± 0.06	0.82	1.02 ± 0.04
Walker2d	1.00 ± 0.02	0.05	0.95 ± 0.18

Table 11. Performance of Vintix, REGENT and JAT on MuJoCo domain tasks.

Task	Vintix	REGENT	JAT (Full Dataset)
assembly	1.04 ± 0.10	0.83	0.96 ± 0.17
basketball	1.02 ± 0.11	0.68	-0.00 ± 0.00
bin-picking	0.01 ± 0.01	0.67	0.47 ± 0.52
box-close	-0.04 ± 0.03	0.93	0.89 ± 0.39
button-press	0.97 ± 0.07	0.62	0.86 ± 0.30
button-press-topdown	0.94 ± 0.14	0.62	0.51 ± 0.17
button-press-topdown-wall	0.97 ± 0.07	0.62	0.53 ± 0.19
button-press-wall	1.00 ± 0.04	0.94	0.94 ± 0.18
coffee-button	1.00 ± 0.06	0.84	0.38 ± 0.41
coffee-pull	0.07 ± 0.20	0.62	0.14 ± 0.27
coffee-push	1.01 ± 0.20	0.18	0.30 ± 0.44
dial-turn	0.99 ± 0.07	0.83	0.95 ± 0.16
disassemble	1.00 ± 0.12	2.24	0.17 ± 3.91
door-close	1.02 ± 0.05	1.00	0.99 ± 0.06
door-lock	0.35 ± 0.36	0.85	0.84 ± 0.28
door-open	0.99 ± 0.05	0.98	0.99 ± 0.10
door-unlock	0.21 ± 0.26	0.90	0.95 ± 0.13
drawer-close	0.96 ± 0.01	1.00	0.64 ± 0.30
drawer-open	1.00 ± 0.01	0.96	0.98 ± 0.10
faucet-close	0.99 ± 0.03	0.53	0.23 ± 0.18
faucet-open	0.97 ± 0.03	0.99	0.70 ± 0.37
hammer	0.97 ± 0.12	0.95	0.96 ± 0.15
hand-insert	0.19 ± 0.20	0.82	0.93 ± 0.25
handle-press	1.00 ± 0.15	0.99	0.84 ± 0.32
handle-press-side	0.99 ± 0.02	0.99	0.01 ± 0.09
handle-pull	1.00 ± 0.02	0.48	0.83 ± 0.25
handle-pull-side	1.00 ± 0.11	0.48	0.50 ± 0.49
lever-pull	0.96 ± 0.16	0.19	0.40 ± 0.43
peg-insert-side	1.01 ± 0.40	0.70	0.81 ± 0.51
peg-unplug-side	0.75 ± 0.34	0.31	0.17 ± 0.32
pick-out-of-hole	0.91 ± 0.20	0.01	0.00 ± 0.00
pick-place	0.98 ± 0.22	0.99	0.32 ± 0.48
pick-place-wall	1.04 ± 0.16	0.99	0.10 ± 0.29
plate-slide	0.99 ± 0.34	1.00	0.90 ± 0.42
plate-slide-back	0.99 ± 0.16	1.00	0.24 ± 0.00
plate-slide-back-side	0.99 ± 0.09	1.00	0.96 ± 0.17
plate-slide-side	0.83 ± 0.22	0.99	0.16 ± 0.04
push	0.97 ± 0.14	0.84	0.94 ± 0.21
push-back	0.95 ± 0.29	0.84	0.97 ± 1.29
push-wall	0.99 ± 0.02	0.81	0.21 ± 0.30
reach	1.01 ± 0.26	0.99	0.34 ± 0.32
reach-wall	0.98 ± 0.17	0.99	0.81 ± 0.37
shelf-place	1.01 ± 0.11	0.96	0.38 ± 0.46
soccer	0.80 ± 0.35	0.61	0.77 ± 0.44
stick-pull	0.92 ± 0.16	0.88	0.92 ± 0.23
stick-push	0.90 ± 0.28	0.75	0.48 ± 0.48
sweep	0.94 ± 0.12	0.91	0.01 ± 0.04
sweep-into	1.00 ± 0.02	0.91	0.99 ± 0.06
window-close	0.95 ± 0.17	0.90	0.67 ± 0.39
window-open	0.96 ± 0.17	0.97	0.98 ± 0.12

Table 12. Performance of Vintix, REGENT and JAT on Meta-World domain tasks.